

CRL4^{AMBRA1} is a master regulator of D-type cyclins

<https://doi.org/10.1038/s41586-021-03445-y>

Received: 8 March 2020

Accepted: 11 March 2021

Published online: 14 April 2021

 Check for updates

Daniele Simoneschi^{1,2}, Gergely Rona^{1,2,3}, Nan Zhou⁴, Yeon-Tae Jeong^{1,2}, Shaowen Jiang^{1,2}, Giacomo Milletti^{5,6}, Arnaldo A. Arbini^{2,7}, Alfie O'Sullivan^{1,2}, Andrew A. Wang^{1,2}, Sorasicha Nithikasem^{1,2}, Sarah Keegan^{1,2,8}, Yik Siu¹, Valentina Cianfanelli^{5,9}, Emiliano Maiani^{9,10}, Francesca Nazio⁵, Francesco Cecconi^{5,6,9}, Francesco Boccalatte^{2,7}, David Fenyö^{1,2,8}, Drew R. Jones¹, Luca Busino⁴✉ & Michele Pagano^{1,2,3}✉

D-type cyclins are central regulators of the cell division cycle and are among the most frequently deregulated therapeutic targets in human cancer¹, but the mechanisms that regulate their turnover are still being debated^{2,3}. Here, by combining biochemical and genetics studies in somatic cells, we identify CRL4^{AMBRA1} (also known as CRL4^{DCAF3}) as the ubiquitin ligase that targets all three D-type cyclins for degradation. During development, loss of *Ambra1* induces the accumulation of D-type cyclins and retinoblastoma (RB) hyperphosphorylation and hyperproliferation, and results in defects of the nervous system that are reduced by treating pregnant mice with the FDA-approved CDK4 and CDK6 (CDK4/6) inhibitor abemaciclib. Moreover, *AMBRA1* acts as a tumour suppressor in mouse models and low *AMBRA1* mRNA levels are predictive of poor survival in cancer patients. Cancer hotspot mutations in D-type cyclins abrogate their binding to *AMBRA1* and induce their stabilization. Finally, a whole-genome, CRISPR–Cas9 screen identified *AMBRA1* as a regulator of the response to CDK4/6 inhibition. Loss of *AMBRA1* reduces sensitivity to CDK4/6 inhibitors by promoting the formation of complexes of D-type cyclins with CDK2. Collectively, our results reveal the molecular mechanism that controls the stability of D-type cyclins during cell-cycle progression, in development and in human cancer, and implicate *AMBRA1* as a critical regulator of the RB pathway.

D-type cyclins (cyclin D1, cyclin D2 and cyclin D3) promote cell proliferation by activating CDK4 and CDK6, which, in turn, phosphorylate and inactivate members of the RB family of proteins¹. To date, seven substrate receptors of CUL1–RING ubiquitin ligases (CRLs) (the F-box proteins FBXO4, FBXO31, β-TrCP, FBXW8, SKP2, FBXL2 and FBXL8) and the anaphase-promoting complex/cyclosome (APC/C) have been proposed to target D-type cyclins for degradation³. However, Kanie et al.² showed that cyclin D1 stability was unaffected in cells depleted of *FBXO4*, *FBXO31*, *FBXW8* and *SKP2* (alone or in combination) or in which CRL1 or APC/C activities were abrogated in the presence or absence of DNA damage. These results suggest the existence of one or more alternative bona fide ubiquitin ligase(s) targeting D-type cyclins.

Three screens for cyclin D1 regulators

Treatment of human cell lines with MLN4924, an inhibitor of all CRLs, induced accumulation and stabilization of D-type cyclins (Extended Data Fig. 1a, b). Silencing of either *CUL4A* and *CUL4B* or their associated subunit *DDB1*, but not other cullins, resulted in the accumulation

of cyclin D1 and cyclin D3, and their phosphorylated forms (Fig. 1a and Extended Data Fig. 1c). Silencing of *CUL1* or expression of a dominant-negative *CUL1* mutant did not affect the levels of D-type cyclins in multiple cell lines (Extended Data Fig. 1d–h). To identify the substrate receptors of CRL4 complexes involved in the degradation of cyclin D1, we performed three orthogonal screens (Fig. 1b). First, we used a short interfering RNA (siRNA) approach in cells stably expressing fluorescently-tagged cyclin D1 (Extended Data Fig. 1i–k). We transfected oligonucleotides targeting all predicted human DDB1–CUL4-associated factors (DCAFs), the substrate receptors of CRL4 complexes⁴, and identified five hits (Fig. 1c). Using this approach, we identified five hits, four of which are shared between the two cell lines tested (*AMBRA1*, *DDA1*, *ERCC8*, and *TORIAIP2*). Notably, silencing of *ERCC8* revealed a peak in the accumulation of cyclin D1 at around 48–54 hours, which decreased at subsequent time points. Of the remaining three hits, silencing of *AMBRA1* showed a consistent accumulation of cyclin D1 over time. Second, we used a proteomics approach, and identified six DCAFs that interacted with wild-type cyclin D1, but not with cyclin D1(T286A), a mutant insensitive to ubiquitin-mediated

¹Department of Biochemistry and Molecular Pharmacology, NYU Grossman School of Medicine, New York, NY, USA. ²Laura and Isaac Perlmutter Cancer Center, NYU Grossman School of Medicine, New York, NY, USA. ³Howard Hughes Medical Institute, NYU Grossman School of Medicine, New York, NY, USA. ⁴Department of Cancer Biology, University of Pennsylvania Perelman School of Medicine, Philadelphia, PA, USA. ⁵Department of Pediatric Hemato-Oncology and Cell and Gene Therapy, IRCCS Bambino Gesù Children's Hospital, Rome, Italy. ⁶Department of Biology, University of Rome Tor Vergata, Rome, Italy. ⁷Department of Pathology, NYU Grossman School of Medicine, New York, NY, USA. ⁸Institute for Systems Genetics, NYU Grossman School of Medicine, New York, NY, USA. ⁹Cell Stress and Survival Unit, Danish Cancer Society Research Center, Copenhagen, Denmark. ¹⁰Computational Biology Laboratory, Danish Cancer Society Research Center, Copenhagen, Denmark. ✉e-mail: businol@upenn.edu; michele.pagano@nyulangone.org

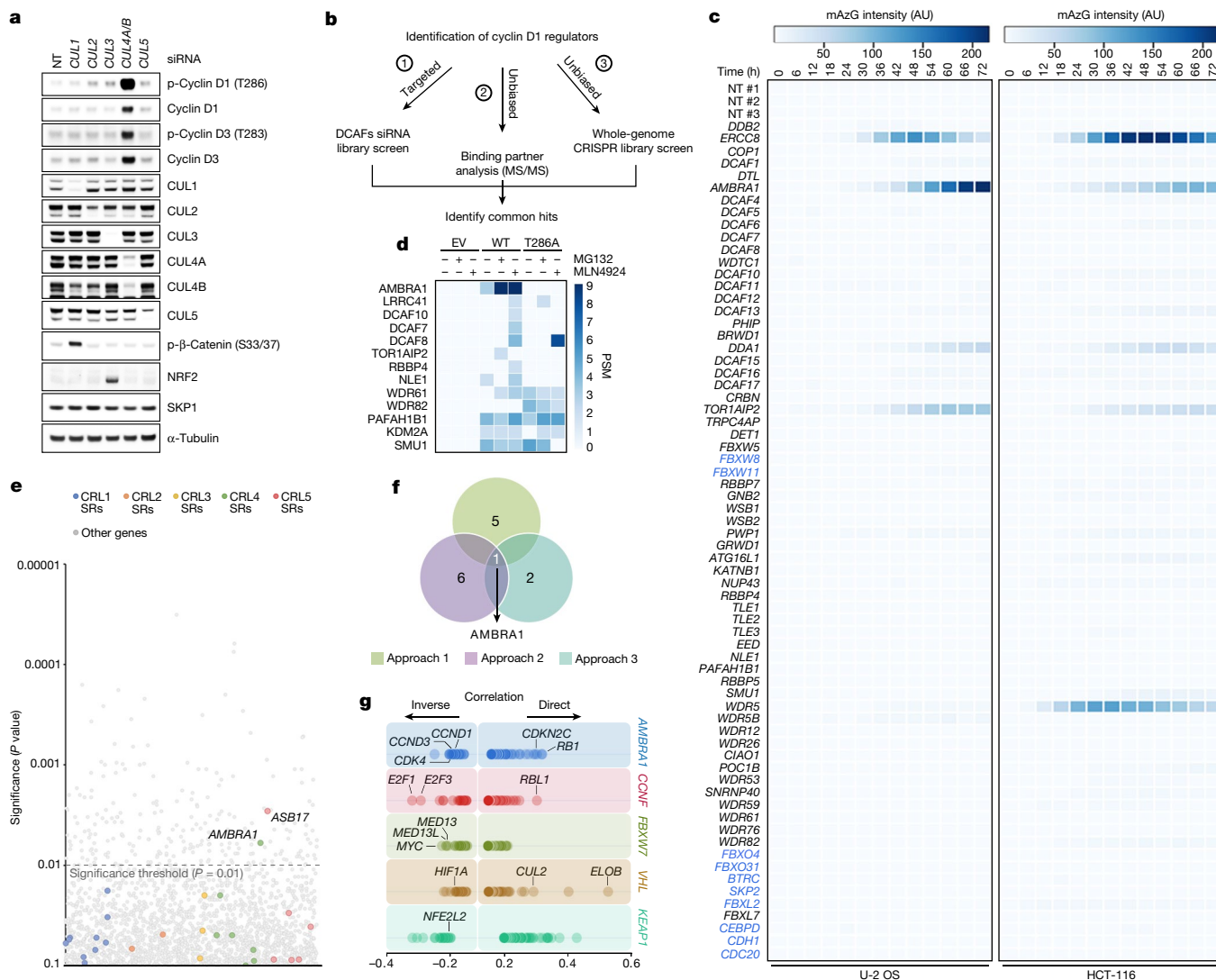


Fig. 1 | Three orthogonal screens identify CRL4^{AMBRA1} as a regulator of cyclin D1. **a**, HCT-116 cells were transfected with a non-targeting (NT) siRNA or siRNAs against *CUL1*, *CUL2*, *CUL3*, *CUL4A* and *CUL4B* (*CUL4A/B*) or *CUL5*, and cell lysates were blotted with the indicated antibodies for proteins and phosphorylated (p-) proteins. This experiment was performed three times. **b**, Schematic representation of three orthogonal screens employed to identify regulators of cyclin D1. **c**, Heat map showing fluorescence intensity values in arbitrary units (AU), related to approach 1 in **b**. Genes encoding for the previously-reported regulators of D-type cyclins³ are reported in blue. This experiment was performed once in HCT-116 and once in U-2 OS cells. **d**, Heat map showing the number of peptide-spectrum matches (PSM) identified by LC-MS/MS matching

substrate receptors from immunoprecipitates of empty vector (EV), wild-type (WT) cyclin D1, or cyclin D1(T286A), related to approach 2 in **b**. The full list of interactors is provided in Supplementary Table 1. **e**, Scatter plot of hits generated using approach 3 in **b**. This experiment was performed once, with three technical replicates. *P* values were calculated using the MAGeCK algorithm¹⁴. SR, substrate receptor. **f**, Venn diagram showing the number of hits obtained from the three screens in **b**. **g**, The top 100 CRISPR (Avana) Public 20Q1 pre-computed associations for *AMBRA1* and selected substrate receptors that have a role in human cancer are depicted on the basis of their dependency profiles at genome scale (<https://depmap.org/portal/>; last accessed January 2020).

degradation³ (Fig. 1d, Extended Data Fig. 1l, Supplementary Table 1). Notably, *AMBRA1* (also known as DCAF3) was the only interactor whose binding to cyclin D1 increased in the presence of MG132 or MLN4924, as expected for a ubiquitin ligase–substrate interaction. Third, we conducted a whole-genome CRISPR–Cas9 screen to identify global regulators of cyclin D1 and found two substrate receptors (Fig. 1e, Extended Data Fig. 1m). We identified *AMBRA1* as the only hit common to all three screens (Fig. 1f).

AMBRA1 targets D-type cyclins for degradation

A genetic interaction between *AMBRA1* and the cyclin D–RB pathway was confirmed using depmap (<https://depmap.org/>) (Fig. 1g). Depletion of *AMBRA1*, but not of any of the other hits or of ubiquitin ligases reported to be involved in the degradation of D-type cyclins³, induced

accumulation and stabilization of endogenous cyclin D1 and cyclin D3 (Fig. 2a, Extended Data Fig. 2a–k). Re-expression of *AMBRA1* in *AMBRA1*^{-/-} cells reduced the levels of D-type cyclins (Extended Data Fig. 2l). We tagged endogenous *AMBRA1* with Flag-tagged minimal auxin-inducible degron (2×Flag–mAID)⁵ in HCT-116 human colon carcinoma cells. In all knock-in clones, auxin rapidly depleted *AMBRA1* and induced cyclin D1 accumulation (Fig. 2b, Extended Data Fig. 3a–c). Auxin washout replenished *AMBRA1*, restoring cyclin D1 and cyclin D3 back to basal levels (Fig. 2c). The effects of *AMBRA1* depletion were not synergistic with proteasome or CRL inhibition, and longer exposures of this or similar experiments revealed the presence of high-molecular-mass bands (Extended Data Fig. 3d–f). Immunopurification of cyclin D1 confirmed that loss of *AMBRA1* prevents the poly-ubiquitylation of cyclin D1 (Fig. 2d). The C termini of D-type cyclins contain a highly conserved TP motif responsible for their ubiquitin-mediated degradation³

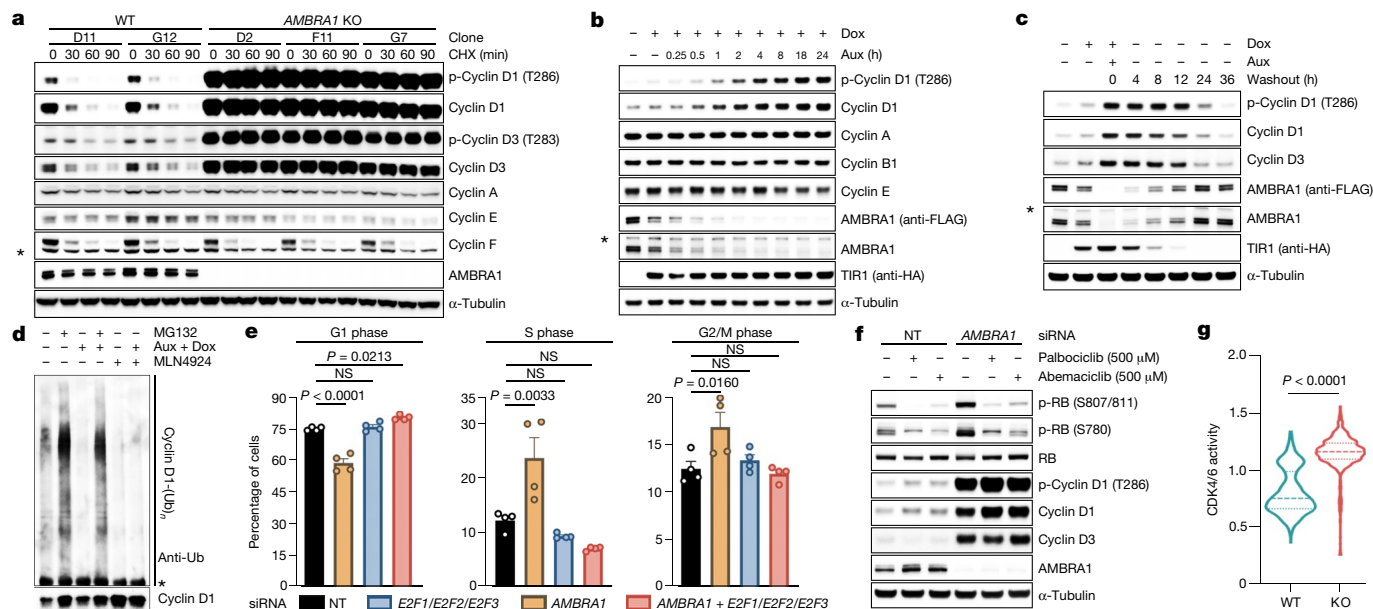


Fig. 2 | AMBRA1 targets D-type cyclins for ubiquitin-mediated degradation, controlling cell cycle progression. **a**, Three *AMBRA1*^{-/-} (KO) and two *AMBRA1*^{+/+} HCT-116 clones were treated with cycloheximide (CHX) as indicated and lysates were blotted with the indicated antibodies. **b**, HCT-116 cells expressing 2×Flag–mAID–AMBRA1 (clone F1) were treated with DMSO or doxycycline (Dox) for 12 h before exposure to auxin (Aux). HA, haemagglutinin. **c**, HCT-116 cells expressing 2×Flag–mAID–AMBRA1 were treated as in **b**, washed, and cultured in growth medium as indicated. **d**, HCT-116 cells expressing 2×Flag–mAID–AMBRA1 were pre-treated with DMSO or doxycycline for 12 h, and exposed to combinations of auxin, doxycycline, MG132 or MLN4924 for 4 h. Endogenous cyclin D1 was immunoprecipitated in denaturing conditions and probed with ubiquitin (Ub) and cyclin D1 antibodies. **e**, HCT-116 cells were transfected with siRNAs as indicated (*E2F1/E2F2/E2F3*,

E2F1, *E2F2* and *E2F3* siRNA; Extended Data Fig. 5h) before pulsing with EdU for 45 min. Cell cycle profiles were measured by flow cytometry. Data are mean ± s.e.m. (*n* = 4 biological replicates per group). Adjusted *P* values were calculated using a one-way ANOVA with Dunnett’s multiple comparisons test. NS, not significant. **f**, HCT-116 cells were transfected with a non-targeting (NT) siRNA or an siRNA against *AMBRA1* before treatment with palbociclib or abemaciclib for 24 h. **g**, Ratio of cytoplasmic to nuclear CDK4/6 activity was measured in individual cells (Extended Data Fig. 5i). Violin plots show median (dashed line) and quartiles (dotted lines). *P* values were calculated using the non-parametric Mann–Whitney, unpaired *t*-test between *AMBRA1* WT (*n* = 642 cells) and *AMBRA1* KO (*n* = 738 cells). Unless otherwise noted, experiments were performed at least three independent times. Asterisks indicate non-specific bands.

(Extended Data Fig. 4a, b). Mutations in this motif impaired the ability of D-type cyclins to interact with AMBRA1, consistent with their stabilization (Extended Data Fig. 4c–g). Cyclin D1 co-precipitated AMBRA1, but not FBXO4, FBXW8 or β-TrCP1, although these three substrate receptors co-precipitated with their respective substrates (Extended Data Fig. 4h–j). Similarly, Kanie et al. could not observe binding of cyclin D1 to FBXO4, FBXW8, β-TrCP1, FBXO31 or CDH1 in the absence or presence of DNA damage². Conversely, we confirmed SKP2–cyclin D1 interaction, but this was independent of T286/P287 (Extended Data Fig. 4c, h), in agreement with the lack of cyclin D1 accumulation upon *SKP2* silencing (Extended Data Fig. 2a, b). AMBRA1–cyclin D1 interaction was confirmed at the endogenous level, and removal of AMBRA1 did not induce accumulation of cyclin D1(T286A) (Extended Data Fig. 4k, l). The ratio of phosphorylated cyclin D1 to total cyclin D1 and the percentage accumulation of phosphorylated cyclin D1 compared with that of total cyclin D1 was higher in AMBRA1-depleted cells than in control cells (Extended Data Fig. 4m, n). Post-translational modification analysis confirmed that K269 is the major site of ubiquitylation in cyclin D1⁶, and revealed the absence of this modification in cyclin D1(T286A) or when cells were treated with MLN4924 (Extended Data Fig. 4o). Incubation of a synthetic cyclin D1 phosphopeptide containing K269 and phosphorylated T286 with in vitro translated AMBRA1 resulted in the formation of higher-molecular-mass bands, which were ubiquitylated species, since they were not present when the phosphopeptide was incubated with ubiquitin(KO) (Extended Data Fig. 4p, q). *AMBRA1* depletion abolished the S-phase degradation of cyclin D1, impaired degradation of D-type cyclins upon nutrient deprivation and genotoxic stress, promoted RB hyperphosphorylation, and induced an E2F-mediated increase in the populations of S and G2/M cells (Fig. 2e–g, Extended Data Fig. 5a–i).

AMBRA1 and cyclin D1 were both detected in the nucleus, and *AMBRA1* depletion accumulated nuclear cyclin D1 (Extended Data Fig. 5j). Lepotomycin B treatment did not stabilize cyclin D1, and cyclin D1 fused to a nuclear-localization signal was destabilized (Extended Data Fig. 5k, l).

AMBRA1 controls D-type cyclins in development

Cyclin D2 degron mutants have been identified in 15 individuals with megalencephaly–polymicrogyria–polydactyly–hydrocephalus (MPPH) syndrome, and have been shown to increase proliferation of neural progenitors (Extended Data Fig. 6a–c, Supplementary Table 2). Loss of *Ambra1* leads to neural tube defects associated with increased cell proliferation and apoptosis, resulting in embryonic lethality⁷. Compared to wild-type mice, *Ambra1*^{fl/fl} mice⁷ displayed accumulation of D-type cyclins, which correlated with an increase in RB phosphorylation and Ki67 levels (Fig. 3a–c, Extended Data Fig. 6d, i–k). We administered abemaciclib to pregnant mice at embryonic day (E)8.5. Targeted liquid chromatography–mass spectrometry (LC-MS/MS) analysis detected the compound in the amniotic fluid and embryonic tissues (Extended Data Fig. 6e–h, Supplementary Figs. 3–5). Abemaciclib treatment decreased RB phosphorylation and rescued the hyperproliferative and neuronal phenotypes, including spina bifida and the overgrowth of telencephalic structures (Fig. 3b–d, Extended Data Fig. 6d, i).

AMBRA1 is a tumour suppressor

Similar to other substrate receptors that act as tumour suppressors, *AMBRA1* displayed a signature of cancer-associated mutations (Extended Data Fig. 7a), which suggests that *AMBRA1* is a

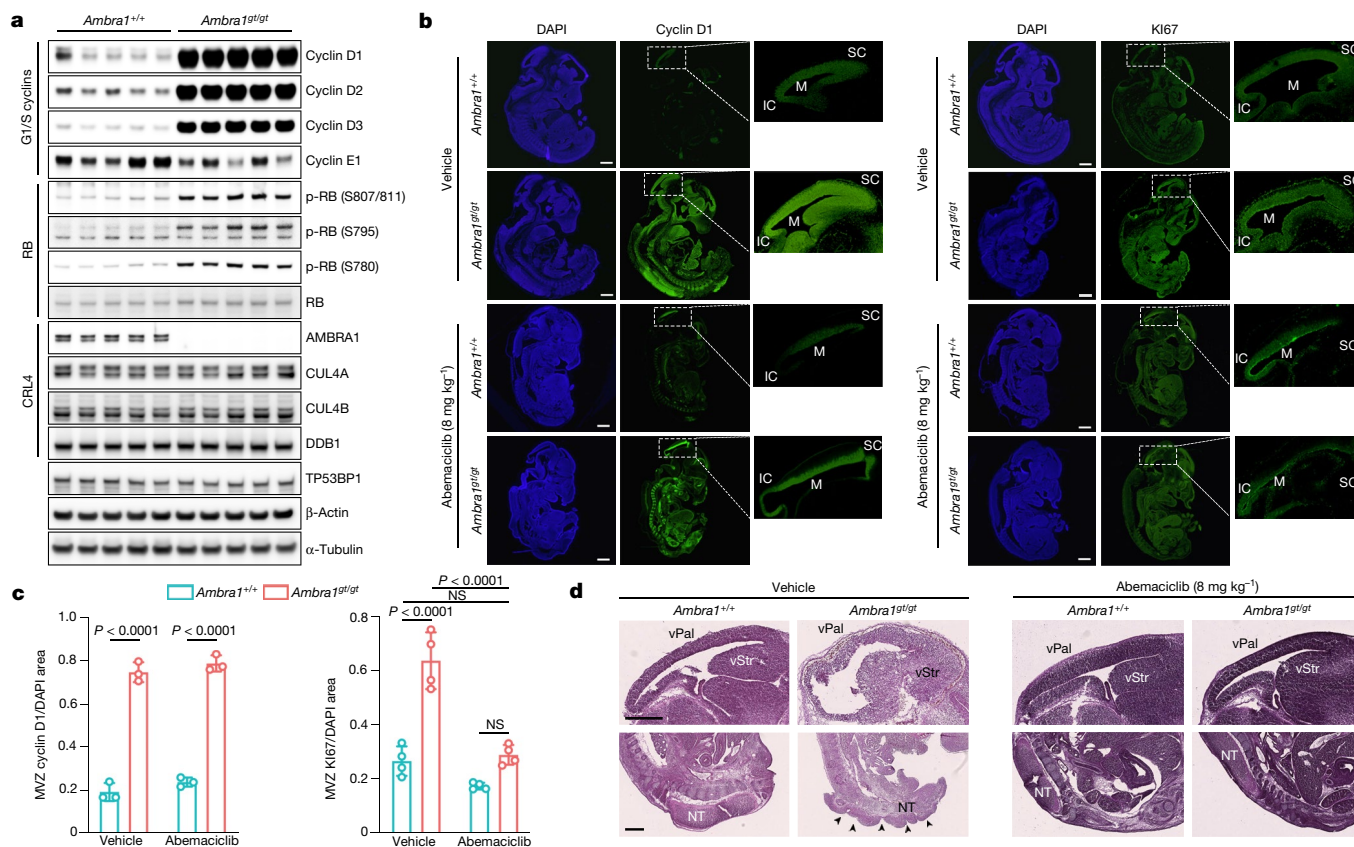


Fig. 3 | D-type cyclins accumulate in *Ambra1*^{Gt/Gt} mice and their hyperproliferative and neurological phenotypes are attenuated by CDK4/6 inhibition. a, Immunoblotting of protein extracts of brain lysates from five E13.5 *Ambra1*^{+/+} and five *Ambra1*^{Gt/Gt} mouse embryos. **b**, Representative immunofluorescent staining of E13.5 *Ambra1*^{+/+} and *Ambra1*^{Gt/Gt} embryos collected from PBS-treated (top two rows) and abemaciclib-treated (bottom two rows) pregnant mice. M, mesencephalic ventricle; SC, superior colliculus; IC, inferior colliculus. Scale bars, 500 μm. **c**, Area of immunofluorescent staining for cyclin D1 and Ki67 in the mesencephalic

ventricular zone (MVZ) (data are mean ± s.d.; cyclin D1 *n* = 3; Ki67 *n* = 4). *P* values by two-way ANOVA with Tukey's multiple comparisons test. **d**, Representative sections stained with haematoxylin and eosin from PBS- (*n* = 3) or abemaciclib-treated (*n* = 7) E13.5 *Ambra1*^{+/+} and *Ambra1*^{Gt/Gt} embryos. Top row, telencephalic structures: vStr (ventricular zone of striatum) and vPal (ventricular zone of pallium). Bottom row, caudal portion of the neural tube (NT). Arrows indicate the spina bifida phenotype. Scale bars, 500 μm. Unless otherwise noted, experiments were performed at least three independent times.

tumour suppressor gene⁸. Analysis of *AMBRA1* mRNA and cyclin D1 protein levels revealed an inverse correlation in several tumour types (results validated by immunohistochemistry), and analysis of The Cancer Genome Atlas (TCGA) dataset (<https://cancer.gov/tcga>) revealed that low *AMBRA1* expression is an unfavourable prognostic marker in several human cancers (Extended Data Fig. 7b–f). D-type cyclins are among the top therapeutic targets in human cancer⁹, and mutations in *CCND1*, *CCND2* and *CCND3* degons have been identified in numerous malignancies (Extended Data Figs. 7g, 8, Supplementary Table 3). To evaluate whether *AMBRA1* could be a tumour suppressor, we focused our studies on diffuse large B-cell lymphoma (DLBCL) because: (1) the large number of mutations in *CCND3* degon in patients with DLBCL (Extended Data Fig. 8); (2) a forward genetic screen identified *Ambra1* as the top putative tumour suppressor gene in DLBCL¹⁰; (3) when we examined the CRISPR gene-score distribution of six human DLBCL cell lines¹¹, *AMBRA1* was among the top tumour suppressor genes (Extended Data Fig. 9); (4) *AMBRA1* mRNA levels are lower in DLBCL than in normal B-lymphocytes (<https://www.oncomine.org/>) (Extended Data Fig. 10a, b); (5) the *AMBRA1* promoter is hypermethylated in DLBCL (Extended Data Fig. 10c); (6) low expression of *AMBRA1* is an unfavourable prognostic marker in DLBCL (Extended Data Fig. 10d). TCGA dataset analysis revealed that mutations in the RB pathway (including in *AMBRA1*) account for 51% of cases (Extended Data Fig. 10e). Moreover, the transcriptional signatures of tumours bearing either deletion/missense mutations in *AMBRA1* or amplifications/

activating mutations in *CCND3* cluster together, and this signature is enriched for genes belonging to E2F-mediated transcription and G1/S processes (Extended Data Fig. 10f,g). Notably, compared to parental cells, *AMBRA1*^{-/-} lymphoma cells displayed a robust stabilization of cyclin D1 and cyclin D3 and generated tumours with increased volume and weight in NSG immunodeficient mice (Extended Data Fig. 10h–l).

***AMBRA1* loss reduces sensitivity to CDK4/6 inhibitors**

We performed a whole-genome, CRISPR–Cas9 screen aimed at identifying regulators of the response to CDK4/6 inhibitors in U-2 OS human osteosarcoma cells treated with palbociclib. *AMBRA1* was identified as the top hit and the results were validated with palbociclib and abemaciclib in three cell lines (Extended Data Fig. 11a–c). Upon abemaciclib treatment, RB was more phosphorylated in *AMBRA1*-depleted cells than in control cells (Extended Data Fig. 11d, e, Fig. 2f). *AMBRA1*-knockout cells displayed increased interactions between D-type cyclins and CDK4, and also between D-type cyclins and CDK2¹² (Fig. 4a, Extended Data Fig. 11f–i). We also observed an increase in the formation of cyclin D1(T286A)–CDK2 complexes (Extended Data Fig. 11j). All three D-type cyclins formed an active complex with CDK2, which, in contrast to complexes with CDK4, were insensitive to palbociclib (Fig. 4b, Extended Data Fig. 12a–c). Silencing of *CDK2* in *AMBRA1*-knockout cells resensitized them to both abemaciclib and palbociclib (Extended Data Fig. 12d, e). Next, we xenotransplanted parental and *AMBRA1*^{-/-} DLBCL cells into

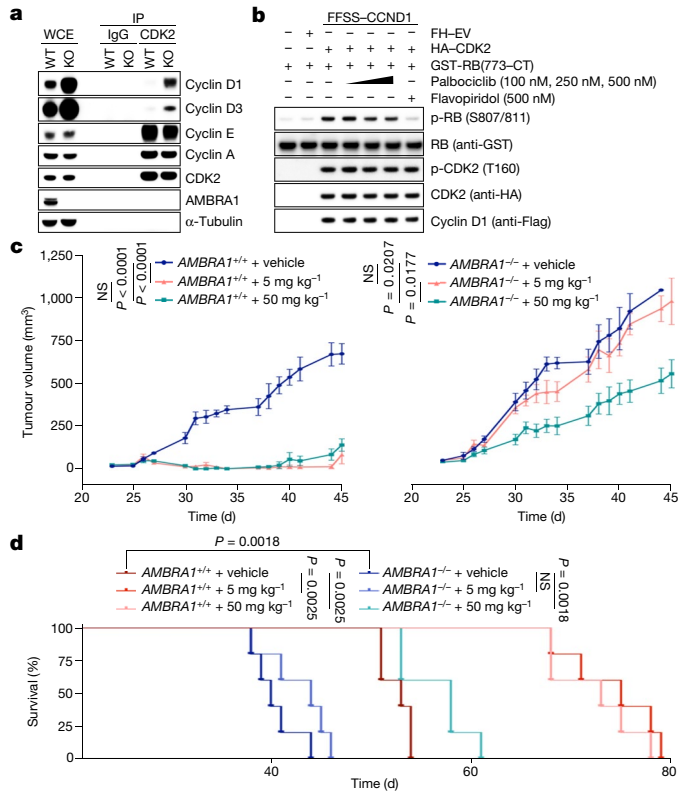


Fig. 4 | AMBRA1 acts as a tumour suppressor and its absence reduces sensitivity to inhibitors of CDK4/6 by promoting the formation of D-type cyclins-CDK2 complexes. **a**, Endogenous CDK2 and IgG control immunoprecipitations (IPs) from parental and *AMBRA1*^{-/-} HCT-116 cells. WCE, whole-cell extracts. **b**, HEK 293T cells were transfected as indicated. Immunopurified cyclin D1-CDK2 complexes were incubated with GST-RB(773-CT) and treated with palbociclib or flavopiridol. CT, C terminus. **c**, **d**, U-2932 cells expressing control short guide RNA (sgRNA) targeting luciferase or *AMBRA1* were subcutaneously xenotransplanted in NSG mice and treated with PBS (vehicle) or palbociclib at the two indicated concentrations. **c**, Tumour volume. Data are mean \pm s.e.m. ($n = 5$ per group at day 0). P values by unpaired, multiple-comparison t -test using the Holm-Sidak's method, calculated at day 45 for the *AMBRA1*^{+/+} group and at day 40 for the *AMBRA1*^{-/-} group (the latest time point where at least 3 mice per group were available). **d**, Survival curves. Experimental end point was declared when tumour volume reached 1,000 mm³ ($n = 5$ per group). P values by log-rank (Mantel-Cox) test. Unless otherwise noted, experiments were performed at least three independent times.

NSG mice, and treated them with palbociclib at two different concentrations. While both doses efficiently reduced the growth of tumours from parental cells, the growth of *AMBRA1*^{-/-} tumours was significantly reduced only when mice were treated with the higher concentration of palbociclib (Fig. 4c). Mice bearing *AMBRA1*^{-/-} tumours had a shorter survival time than those bearing tumours from parental cells, and whereas both doses extended the survival of the mice bearing tumours from parental cells, the mice bearing *AMBRA1*^{-/-} tumours were affected only by the higher concentration of palbociclib (Fig. 4d).

Discussion

Our study shows that CRL4^{AMBRA1} is the ubiquitin ligase that acts during normal cell cycle progression, as well as upon nutrient deprivation and genotoxic stress, to target all three D-type cyclins for ubiquitin-mediated degradation (Extended Data Fig. 12f). Moreover, our findings agree with previous studies that could not confirm a role for CRL1s and APC/C^{2,3} in the ubiquitin-mediated degradation of D-type cyclins. RB ensures proper neurogenesis and acts as a tumour suppressor¹. Similarly, we found that, by regulating the degradation of D-type cyclins, AMBRA1 also warrants proper neurodevelopment and acts as a tumour suppressor in vivo. We also propose that decreased levels of AMBRA1 may be one of the mechanisms of desensitization to CDK4/6 inhibitors, not only by increasing the formation of D-type cyclins-CDK4/6 complexes, but also by increasing the formation of complexes with CDK2, which are insensitive to CDK4/6 inhibitors. Overall, these data highlight the need for the development of inhibitors that simultaneously target CDK2, CDK4 and CDK6, while avoiding the toxic inhibition of CDK1¹³.

Online content

Any methods, additional references, Nature Research reporting summaries, source data, extended data, supplementary information, acknowledgements, peer review information; details of author contributions and competing interests; and statements of data and code availability are available at <https://doi.org/10.1038/s41586-021-03445-y>.

- Malumbres, M. & Barbacid, M. Cell cycle, CDKs and cancer: a changing paradigm. *Nat. Rev. Cancer* **9**, 153–166 (2009).
- Kanie, T. et al. Genetic reevaluation of the role of F-box proteins in cyclin D1 degradation. *Mol. Cell. Biol.* **32**, 590–605 (2012).
- Qie, S. & Diehl, J. A. Cyclin D degradation by E3 ligases in cancer progression and treatment. *Semin. Cancer Biol.* **67**, 159–170 (2020).
- Reichermeier, K. M. et al. PIKES analysis reveals response to degraders and key regulatory mechanisms of the CRL4 network. *Mol. Cell* **77**, 1092–1106.e9 (2020).
- Natsume, T., Kiyomitsu, T., Saga, Y. & Kanemaki, M. T. Rapid protein depletion in human cells by auxin-inducible degron tagging with short homology donors. *Cell Rep.* **15**, 210–218 (2016).
- Barbash, O., Egan, E., Pontano, L. L., Kosak, J. & Diehl, J. A. Lysine 269 is essential for cyclin D1 ubiquitylation by the SCF^{Fbx4/ub-crystallin} ligase and subsequent proteasome-dependent degradation. *Oncogene* **28**, 4317–4325 (2009).
- Fimia, G. M. et al. Ambr1 regulates autophagy and development of the nervous system. *Nature* **447**, 1121–1125 (2007).
- Davoli, T. et al. Cumulative haploinsufficiency and triplosensitivity drive aneuploidy patterns and shape the cancer genome. *Cell* **155**, 948–962 (2013).
- Behan, F. M. et al. Prioritization of cancer therapeutic targets using CRISPR-Cas9 screens. *Nature* **568**, 511–516 (2019).
- Rahrmann, E. P. et al. *Sleeping Beauty* screen identifies *RREB1* and other genetic drivers in human B-cell lymphoma. *Mol. Cancer Res.* **17**, 567–582 (2019).
- Reddy, A. et al. Genetic and functional drivers of diffuse large B cell lymphoma. *Cell* **171**, 481–494 (2017).
- Chytil, A. et al. Construction of a cyclin D1-Cdk2 fusion protein to model the biological functions of cyclin D1-Cdk2 complexes. *J. Biol. Chem.* **279**, 47688–47698 (2004).
- Asghar, U., Witkiewicz, A. K., Turner, N. C. & Knudsen, E. S. The history and future of targeting cyclin-dependent kinases in cancer therapy. *Nat. Rev. Drug Discov.* **14**, 130–146 (2015).
- Li, W. et al. MAGECK enables robust identification of essential genes from genome-scale CRISPR/Cas9 knockout screens. *Genome Biol.* **15**, 554 (2014).

Publisher's note Springer Nature remains neutral with regard to jurisdictional claims in published maps and institutional affiliations.

© The Author(s), under exclusive licence to Springer Nature Limited 2021

Article

Methods

No statistical methods were used to predetermine sample size. The experiments were not randomized except that NSG mice were matched by age, and randomly assigned to specific treatment groups. No blinding was performed in experimental mouse interventions as knowledge of the treatment groups was required. Generally, the investigators were not blinded to allocation during experiments and outcome assessment, except when samples were assigned number labels, and randomized in order to remove downstream operator bias.

Cell culture

Cell lines were purchased from ATCC, except where indicated, and routinely monitored for *Mycoplasma* contamination using the Universal Mycoplasma Detection Kit (ATCC 30-1012K). HEK 293T (ATCC CRL-3216), hTERT RPE-1 (ATCC CRL-4000), T98G (ATCC CRL-1690) and NIH/3T3 (ATCC CRL-1658) cells were maintained in Dulbecco's modified Eagle's medium (DMEM) (Gibco). HCT-116 (ATCC CCL-247) and U-2 OS (ATCC HTB-96) cells were maintained in McCoy's 5A medium (Gibco). PC-3 (ATCC CRL-1435), BJAB and U-2932 cells (both kindly provided to L.B. by A. Thomas-Tikhonenko, Y. Yang and L. Pasqualucci) were maintained in RPMI 1640 medium (Gibco), supplemented with 1 mM sodium pyruvate (Gibco). All media were supplemented with 10% fetal bovine serum (FBS) (Corning Life Sciences) and 1% penicillin/streptomycin/L-glutamine (Corning Life Sciences). HCT-116 2×Flag-mAID-AMBRA1 cells stably infected with pTRIPZ-HA-TIR1 were maintained in McCoy's 5A medium supplemented with 10% Tet System Approved FBS (Takara, Clontech Laboratories) and 1% penicillin/streptomycin/L-glutamine (Corning Life Sciences). All cell lines were maintained at 37 °C and 5% CO₂ in a humidified atmosphere. Where indicated, cells were treated with 0.1 mg ml⁻¹ bafilomycin A1 (Santa Cruz Biotechnology), 20 μM chloroquine (Sigma-Aldrich), 100 μg ml⁻¹ cycloheximide (Sigma-Aldrich), 0.4 μg ml⁻¹ doxycycline (Sigma-Aldrich), 10 μM EdU (Thermo Fisher Scientific), 0.1 mM indole-3-acetic acid (auxin, Sigma-Aldrich), 20 nM leptomycin B (Cell Signaling), 10 μM MMG132 (Peptides International) and 2.5 μM MLN4924 (Active Biochem). Where indicated, cells were nutrient deprived in Earle's Balanced Salt Solution (EBSS) (Sigma-Aldrich) for 4 h before collection. Where indicated, cells were exposed to 5 mJ cm⁻² UV irradiation for the indicated time points before collection.

Plasmids and antibodies

Homo sapiens cDNAs were amplified by PCR using Q5 High Fidelity DNA Polymerase (New England Biolabs) and sub-cloned into a variety of vector backbones, including modified pCDNA3.1 vectors containing N-terminal Flag, HA or Strep tags, pBABE-PURO retroviral vectors containing N-terminal Flag, HA, Strep, mAzG, eGFP or mPlum tags, pMSCV-PURO retroviral vectors containing N-terminal Flag or Strep tags, and pLVX-IRES-PURO or pLVX-IRES-mCherry lentiviral vectors containing N-terminal Flag or Strep-tags. FFSS indicates a tandem 2×Flag–2×Strep tag; SF indicates a Strep–Flag tag. lentiCas9-Blast was a gift from F. Zhang (Addgene plasmid # 52962)¹⁵. Site-directed mutagenesis was performed using KAPA HiFi DNA Polymerase (Kapa Biosystems). The following antibodies were used: β-actin (1:5,000, Sigma-Aldrich A5441), AMBRA1 (1:1,000, Proteintech Group 13762-1-AP), AMBRA1 (1:1,000, Santa Cruz Biotechnology sc-398204), AMBRA1 (1:1,000, Millipore ABC131), p-ATM (S1981) (1:1,000, Cell Signaling Technology 4526L), β-TrCP1 (1:1,000, Cell Signaling Technology 4394S), p-β-catenin (S33-37) (1:1,000, Cell Signaling Technology 9561S), CDC6 (1:1,000, Santa Cruz Biotechnology sc-9964), CDC20 (1:1,000, Cell Signaling Technology 4823S), CDK2 (1:1,000, Bethyl Laboratories A301-812A), p-CDK2 (T160) (1:1,000, Cell Signaling Technology 2561S), CDK4 (1:2,000, M.P. laboratory), CDT1 (1:1,000, Abcam ab70829), p-CHK1 (S317) (1:1,000, Cell Signaling Technology 2344S), p-CHK2 (T68) (1:1,000, Cell Signaling Technology 2661S), CUL1 (1:1,000, Life Technologies 71-8700), CUL2 (1:2,000, Bethyl Laboratories A302-475A),

CUL3 (1:1,000, Bethyl Laboratories A301-109A), CUL4A (1:1,000, Bethyl Laboratories A300-739A), CUL4B (1:1,000, Bethyl Laboratories A303-863A), CUL5 (1:1,000, Bethyl Laboratories, A302-173A), cyclin A (1:5,000, M.P. laboratory), cyclin B1 (1:5,000, M.P. laboratory), cyclin D1 (1:1,000, Abcam ab16663), cyclin D1 (1:1,000, Santa Cruz Biotechnology sc-20044), cyclin D1 (1:1,000, Abcam ab134175), p-cyclin D1 (T286) (1:1,000, Cell Signaling Technology 3300S), cyclin D2 (1:1,000, Cell Signaling Technology 3741S), cyclin D3 (1:1,000, Thermo Fisher Scientific MA5-12717), p-cyclin D3 (T283) (1:1,000, Cell Signaling Technology 53966S), cyclin E (1:1,000, Santa Cruz Biotechnology sc-247), cyclin F (1:1,000, Santa Cruz Biotechnology sc-952), DCAF7 (1:1,000, Novus Biologicals NBP1-92589), DCAF8 (1:1,000, Bethyl Laboratories A301-556A), DDA1 (1:2,000, Proteintech Group 14995-1-AP), DDB1 (1:2,000, Bethyl Laboratories A300-462A), E2F1 (1:1,000, Cell Signaling Technology 3742S), E2F2 (1:1,000, Santa Cruz Biotechnology sc-632), E2F3 (1:1,000, GeneTex GTX11843), EMI1 (1:1,000, Proteintech Group 10872-1-AP), FBXO4 (1:1,000, Santa Cruz Biotechnology sc-376372), FBXO22 (1:1,000, GeneTex GTX117774), Flag (1:2,000, Sigma-Aldrich F1804), Flag (1:2,000, Sigma-Aldrich F7425), FZRI (also known as CDH1, 1:1,000, Thermo Fisher Scientific 34-2000), GST (1:5,000, GE Healthcare 27457701), HA (1:2,000, Bethyl Laboratories A190-108A), LC-3 (1:5,000, Novus Biological NB100-2220), mAID (1:1,000, MBL International M214-3), NeuN (1:1,000, Cell Signaling Technology 24307S), NRF2 (1:1,000, Cell Signaling Technology 12721S), p21 (1:1,000, Cell Signaling Technology 2947S), p27 (1:1,000, BD Biosciences 610241), p53 (1:2,000, Santa Cruz Biotechnology sc-6243), p62 (1:5,000, MBL International PM045), RB (1:1,000, Cell Signaling Technology 9313S), RB (1:1,000, Cell Signaling Technology 9309S), p-RB (S780) (1:1,000, Cell Signaling Technology 8180S), p-RB (S780) (1:1,000, Cell Signaling Technology 9307S), p-RB (S795) (1:1,000, Cell Signaling Technology 9301S), p-RB (S807/811) (1:1,000, Cell Signaling Technology 8516S), p-RB (S807/811) (1:1,000, Cell Signaling Technology 9308S), RRM2 (1:1,000, Cell Signaling Technology 65939S), SKP1 (1:5,000, M.P. laboratory), SKP2 (1:1,000, Santa Cruz Biotechnology sc-1567), Tau (1:1,000, Invitrogen 13-6400), TP53BP1 (1:2,000, Abcam ab36823), α-tubulin (1:5,000, Sigma-Aldrich T6074), β-III tubulin (1:2,000, Invitrogen 480011), ubiquitin (1:1,000, Cell Signaling Technology 3933S).

Transient transfections and virus-mediated gene transfer

For gene silencing, ON-TARGETplus SMARTpool siRNA oligonucleotides (see Supplementary Table 4 for sequence details) were transfected using Lipofectamine RNAiMAX Reagent (Thermo Fisher Scientific), according to the manufacturer's instructions. To achieve satisfactory RNAi-mediated depletion, siRNA oligonucleotides were transfected over two or three rounds. Plasmids were transiently transfected using Lipofectamine 3000 (Thermo Fisher Scientific), according to the manufacturer's instructions, except for HEK 293T cells, which were transfected using polyethylenimine (PEI) (Polysciences). For retrovirus production, HEK 293T cells were transfected with pBABE or pMSCV vectors containing the genes of interest, in combination with pCMV-Gag-Pol and pCMV-VSV-G plasmids. For lentivirus production, HEK 293T cells were transfected with pLentiCRISPR, pLVX, or pTRIPZ vectors containing the genes of interest, in combination with pCMV delta R8.2 and pCMV-VSV-G. The virus-containing medium was collected 48 h after transfection, filtered using 0.22-μm sterile Millex-HV filter units (Millipore Sigma), and supplemented with 8 μg ml⁻¹ polybrene (Sigma). Cells were infected by replacing their culture medium with the virus-containing medium for 8 h. Selection of transduced cells was carried out using either 1 μg ml⁻¹ puromycin (Sigma), 10 μg ml⁻¹ blasticidin S (Gibco) or FACS, depending on the vector selectable marker.

Quantitative PCR with reverse transcription

RNA extraction, reverse transcription and quantitative PCR reactions were performed as previously described¹⁶. In brief, total RNA was extracted using RNeasy Mini Kit (QIAGEN). cDNA was generated

using RNA to cDNA EcoDry Premix (Double Primed) (Takara/Clontech Laboratories) according to manufacturer's instruction. The quantitative PCR reaction was carried out using PowerUp SYBR Green (Thermo Fisher Scientific) with the Thermo Fisher QuantStudio 3 Real-Time PCR system in a 96-well format. ROX was used as a reference dye for fluorescent signal normalization and well-to-well optical variations correction. Bar graphs represent the relative ratios of target genes to housekeeping gene values. See Supplementary Table 4 for primer sequence details.

RNAi library screen

A RNAi ON-TARGETplus SMARTpool Cherry-pick Library was purchased from Dharmacon/Horizon Discovery, including oligonucleotides targeting all DCAF genes¹⁷ (see Supplementary Table 4 for details). The library was resuspended in 1× siRNA Buffer (Dharmacon, Horizon Discovery) to a final 2 μM stock concentration. HCT-116 and U-2 OS cells, previously transduced with pBabe-mAzG-CCND1, were reverse transfected in a 96-well plate with siRNA:DharmaFECT 2 (Dharmacon, Horizon Discovery) complex using 20 nM siRNA and 0.1 μl of DharmaFECT 2 per well, according to the manufacturer's instructions. siRNA:DharmaFECT 2 was complexed in Opti-MEM (Thermo Fisher Scientific). Cells were seeded in FluoroBrite DMEM (Thermo Fisher Scientific) supplemented with 10% FBS (Corning Life Sciences) and 1% penicillin/streptomycin/L-glutamine (Corning Life Sciences). Images were acquired every 6 h for a total of 72 h using a Cytation 5 Imaging Reader (BioTek), equipped with a humidified BioSpa 8 Automated Incubator (BioTek) set at 37 °C and 5% CO₂. Phase contrast imaging was used to generate a cell mask. Total fluorescence intensity was calculated at each time point within the cell mask, and normalized to the first time point (time = 0). Images were analysed with Gen5 (version 3.0).

Immunoprecipitation and immunoblotting

HEK 293T cells were transiently transfected using PEI (Polysciences); HCT-116 and U-2 OS were transiently transfected with Lipofectamine 3000 (Thermo Fisher Scientific). Where indicated, 48 h after transfection, cells were treated with MG132 or MLN4924 for 4 h before collection. Cells were collected and lysed in lysis buffer (50 mM Tris-Cl pH 7.5, 150 mM NaCl, 10% glycerol, 1 mM EDTA, 1 mM EGTA, 5 mM MgCl₂ and 0.2% NP-40), supplemented with protease inhibitors (Complete ULTRA, Roche), phosphatase inhibitors (PhosSTOP, Roche), and 1 mM 1,4-dithiothreitol (DTT) (Sigma-Aldrich). The insoluble fraction was removed by centrifugation (20,000g) for 15 min at 4 °C. Protein concentrations in cell lysates were normalized using the Pierce BCA Protein Assay Kit (Thermo Fisher Scientific), according to the manufacturer's instructions. Immunoprecipitations of Flag-tagged proteins (including endogenous 2×Flag-mAID-AMBRA1) were carried out using Flag-M2 agarose beads (Sigma-Aldrich) for 2 h at 4 °C. The beads were then washed 4 times in lysis buffer and elution of the precipitated complexes was carried out using 3×Flag peptide (Sigma-Aldrich). For denaturing immunoprecipitation of endogenous cyclin D1, HCT-116 cells were collected and lysed with lysis buffer supplemented with 1% SDS. The lysates were boiled for 10 min. The lysates were then diluted with lysis buffer to 0.1% SDS. Cyclin D1 was immunoprecipitated for 2 h at 4 °C using an anti-cyclin D1 antibody (1:50, Abcam Cat. No. ab16663) mixed with Dynabeads Protein G (Thermo Fisher Scientific). Mouse IgG isotype (Thermo Fisher Scientific) was used as a negative control. Endogenous immunoprecipitations of cyclin D1, cyclin D3, CDK2 and CDK4 were carried out for 2 h at 4 °C using anti-cyclin D1 (1:100, Abcam ab134175), anti-cyclin D3 (1:50, Santa Cruz Biotechnology sc-6283), anti-CDK2 (1:100, Bethyl Laboratories A301-812A) and anti-CDK4 (1:100, M.P. Laboratory) antibodies, respectively. For downstream immunoblotting, immunoprecipitates were eluted in NuPAGE LDS sample buffer (Thermo Fisher Scientific) supplemented with β-mercaptoethanol (Sigma-Aldrich) and incubated at 95 °C for 5 min. Whole-cell lysates and immunoprecipitates were separated by SDS-PAGE and transferred to

0.45-μm Immobilon-P PVDF membranes (Millipore Sigma) for western blotting. Transfer efficiency and equal protein amounts or loading were verified by Ponceau S (Sigma-Aldrich) staining. For the immunoblotting of multiple protein targets, membranes were cut into strips corresponding to the target's molecular mass using a Feather Disposable Scalpel (Thermo Fisher Scientific), and containing at least one molecular weight marker. Membranes were then blocked in 5% milk/TBST for 1 h at room temperature and incubated with the indicated primary antibodies at 4 °C overnight. For enhanced chemiluminescence, the detection of proteins was accomplished using the appropriate secondary antibodies conjugated to horseradish peroxidase (anti-mouse and anti-rabbit, GE Healthcare Life Sciences; anti-goat, Santa Cruz Biotechnology) at a 1:5,000 dilution in 5% milk/TBST for 1 h at room temperature. Immunoblots were developed using SuperSignal enhanced chemiluminescence (Thermo Fisher Scientific) using the ImageQuant LAS 4000 (GE Healthcare Life Sciences) image analyser. For fluorescent western blotting, proteins were detected with the appropriate fluorescently labelled, secondary antibodies (IRDye 680RD and IRDye 800CW, LI-COR) at a 1:10,000 dilution in 5% milk/TBST for 1 h at room temperature. Fluorescent western blot signals were detected using the ChemiDoc MP Imaging System (Bio-Rad). Western blot images were acquired with a linear or sigmoid gradation conversion curve. When necessary, membranes were stripped with stripping buffer (Restore PLUS Western Blot Stripping Buffer, Thermo Scientific) for 15 min at room temperature, and reblotted with a different primary antibody. Stripping efficiency was confirmed by redeveloping the membranes after incubation with the stripping buffer (see Supplementary Fig. 6 for example). Images were assembled and rescaled using Adobe Photoshop (version 21.1.0).

Mass spectrometry for proteomics

The immunoprecipitated samples were filtered with Ultrafree centrifugal filters (Millipore Sigma) and concentrated using Amicon Ultra 3,000 NMWL centrifugal filters (Millipore Sigma), according to the manufacturer's instructions. The samples were then resuspended in NuPAGE LDS Sample Buffer (Novex). The proteins were reduced with 2 μl of 0.2 M DTT for 1 h at 57 °C at pH 7.5. Next, the proteins were alkylated with 2 μl of 0.5 M iodoacetamide (Sigma) for 45 min at room temperature in the dark. The samples were loaded on a NuPAGE 4–12% Bis-Tris Gel 1.0 mm (Life Technologies) and run for 20 min at 200 V. The gel was stained with GelCode Blue Stain Reagent (Thermo Fisher Scientific). The gel lanes were excised, cut into 1 mm³ pieces and destained for 15 min in a 1:1 (v/v) solution of methanol and 100 mM ammonium bicarbonate. The buffer was exchanged and the samples were destained for another 15 min. This was repeated for another 3 cycles. The gel plugs were dehydrated by washing with acetonitrile, and further dried by placing them in a SpeedVac for 20 min. 500 ng of sequencing grade modified trypsin (Promega) was added directly to the dried gel pieces followed by enough 100mM ammonium bicarbonate to cover the gel pieces. The gel plugs were allowed to shake at room temperature and digestion proceeded overnight. The digestion was halted by adding a slurry of R2 50 μm Poros beads (Applied Biosystems) in 5% formic acid and 0.2% trifluoroacetic acid (TFA) to each sample at a volume equal to that of the ammonium bicarbonate added for digestion. The samples were allowed to shake at 4 °C for 120 min. The beads were loaded onto C18 ziptips (Millipore Sigma), equilibrated with 0.1% TFA, using a microcentrifuge for 30 s at 6,000 rpm. The beads were washed with 0.5% acetic acid. Peptides were eluted with 40% acetonitrile in 0.5% acetic acid followed by 80% acetonitrile in 0.5% acetic acid. The organic solvent was removed using a SpeedVac concentrator and the sample reconstituted in 0.5% acetic acid. Each sample was loaded onto a trap column (Acclaim PepMap 100 pre-column, 75 μm × 2 cm, C18, 3 μm, 100 Å, Thermo Scientific) connected to an analytical column (EASY-Spray column, 50 m × 75 μm internal diameter, PepMap RSLC C18, 2 μm, 100 Å, Thermo Scientific) using the autosampler of an Easy nLC 1000 (Thermo

Article

Fisher Scientific) with solvent A consisting of 2% acetonitrile in 0.5% acetic acid and solvent B consisting of 80% acetonitrile in 0.5% acetic acid. The peptide mixture was gradient eluted into the Orbitrap Lumos mass spectrometer (Thermo Fisher Scientific) using the following gradient: a 2–31% solvent B in 60 min, 31–40% solvent B in 10 min, followed by 40–100% solvent B in 10 min. The samples were acquired on the Orbitrap Lumos using the following parameters: full MS spectra resolution of 120,000 (at m/z 200), an AGC target of 4×10^5 , maximum ion time of 50 ms, scan range from 400 to 1,500 m/z . Following each full MS scan, low resolution MS/MS spectra were acquired using the TopSpeed algorithm for a 3 s duty cycle. The MS/MS spectra were collected in the ion trap in rapid scan mode, with an AGC target of 1×10^4 , maximum ion time of 30 ms, one microscan, 2 m/z isolation window, normalized collision energy of 32 and a dynamic exclusion of 30 s. To identify binding partners, all acquired MS2 spectra were searched against a UniProt human database using Sequest HT within Proteome Discoverer 1.4 (Thermo Fisher Scientific). The search parameters were as follows: precursor mass tolerance ± 10 ppm, fragment mass tolerance ± 0.02 Da, digestion parameters trypsin allowing two missed cleavages, fixed modification of carbamidomethyl on cysteine, variable modification of oxidation on methionine, and variable modification of deamidation on glutamine and asparagine and a 1% peptide and protein false discovery rate searched against a decoy database. The results were filtered to only include proteins identified by at least two unique peptides. To quantify the post-translational modification sites, the MS/MS spectra were searched against a given protein sequence of interest using Byonic¹⁸ (Protein Metrics). The mass tolerance was set to 10 ppm for MS1 and 0.4 Da for MS2 searches. A false discovery rate of 1% was applied on the protein level. The Byonic search included fixed modification of carboxymethyl on cysteine and variable modifications of oxidation on methionine, ubiquitination at lysine and phosphorylation at serine, threonine and tyrosine residues. The spectra of the peptides of interest were manually verified to localize the phosphorylation and ubiquitination sites. For relative quantification of the modified sites the semi-automatic program Byologic (Protein Metrics) was used to obtain the area under the curve (AUC) for the extracted ion chromatogram of each peptide isoform. The AUC was manually verified and adjusted if appropriate for each isoform. The percent modification was obtained by dividing the isoform AUC by the total AUC for the peptide.

Whole-genome CRISPR–Cas9 screens

HCT-116 (previously transduced with pBabe-mAzG-CCND1) and U-2 OS cells were transduced with lentiCas9-Blast, a gift from F. Zhang (Addgene plasmid #52962)¹⁵, and selected with $10 \mu\text{g ml}^{-1}$ blasticidin S (Gibco). The Human GeCKOv2 CRISPR-knockout pooled library was a gift from F. Zhang (Addgene #1000000049). The library was amplified according to the amplification protocol provided by the F. Zhang laboratory (https://media.addgene.org/cms/filer_public/b5/fd/b5fde702-d02c-4873-806f-24ac28b2a15a/geckov2_library_amplification_protocol_1.pdf) and deep sequenced using Illumina MiSeq (80 cycles forward read + 8 bp for the index read) to verify representation and pool complexity. To produce lentivirus, HEK 293T cells were seeded in twenty, 15-cm dishes and co-transfected with the lentiGuide-Puro plasmid library, pCMV delta R8.2 and pCMV-VSV-G. After 48 h, the supernatant was filtered using 0.22- μm sterile Millex-HV filter units (Millipore Sigma), concentrated by ultracentrifugation at 24,000 rpm for 2 h at 4 °C, and resuspended in DMEM supplemented with 10% FBS. Aliquots were stored at -80 °C. To achieve a multiplicity of infection of 0.3–0.5, 3×10^6 HCT-116 and U-2 OS cells were tested by spinfecting in a 12-well plate with different volumes of virus supplemented with $8 \mu\text{g ml}^{-1}$ polybrene (Sigma). The next day, each well was split into two replicate wells. To calculate percent transduction, one duplicate well was treated with $1 \mu\text{g ml}^{-1}$ puromycin (Sigma) for 3 days. Percent transduction was calculated as cell count from the puromycin-treated cells divided by the cell count from untreated cells multiplied by 100. The

volume of virus which gave a multiplicity of infection of 0.4 was chosen for large-scale screening. For the identification of genes involved in the regulation of cyclin D1, 1×10^8 HCT-116 (previously transduced with pBabe-mAzG-CCND1 and lentiCas9-Blast) were spinfecting as described above, seeding 3×10^6 cells per well in 12-well plates. The day after spinfection, wells were pooled in larger 15-cm dishes and selected for 3 days with $1 \mu\text{g ml}^{-1}$ puromycin (Sigma). To select for guide RNAs (gRNAs) that induced an increase in the levels of fluorescently-tagged cyclin D1, cells were split into two groups. One group was used as reference, while the second group was sorted by FACS to enrich for cells that expressed high levels of mAzG as compared to parental cells not infected with the CRISPR–Cas9 library. Cells were cultured for seven additional days and genomic DNA was extracted with a Blood & Cell Culture Midi kit (QIAGEN). For the identification of genes whose loss confers resistance to palbociclib, 1×10^8 U-2 OS cells (previously transduced with lentiCas9-Blast) were spinfecting as described above, seeding 3×10^6 cells per well in 12-well plates. The day after spinfection, wells were pooled in larger 15-cm dishes and selected for 3 days with $1 \mu\text{g ml}^{-1}$ puromycin (Sigma). Cells were then split into two groups. One group was treated with 500 nM palbociclib (Sigma-Aldrich) for 60 days, while the other group was treated with vehicle (DMSO). Genomic DNA was extracted with a Blood & Cell Culture Midi kit (QIAGEN). For each sample we performed 15 separate PCR reactions using NEBNext Q5 Hot Start HiFi PCR Master Mix (New England Biolabs) (see Supplementary Table 4 for primer details). PCR products were loaded onto an agarose gel, purified, mixed and quantified. Pooled libraries were sequenced on a NextSeq 500 (Illumina), either a mid-output or a high-output cartridge, as single read 81, and index read of 8, PhiX spike-in, 20%. Illumina primers were used as sequencing primers. Upon demultiplexing, FASTQ files were processed and trimmed using Cutadapt (<https://doi.org/10.14806/ej.17.1.200>) to retrieve the unique sgRNA sequence. sgRNA reads were aligned to the library using the MAGECK algorithm¹⁴.

CRISPR–Cas9 genome editing

CRISPR–Cas9 genome editing techniques were carried out as previously described^{19–21}. In brief, to generate *AMBRA1*-knockout cells, optimal gRNA target sequences closest to the genomic target site were designed using the Benchling CRISPR Genome Engineering tool (<https://www.benchling.com>). To generate 2 \times Flag-mAID-*AMBRA1* knock-in HCT-116 cells, an optimal gRNA target sequence closest to the genomic target site and a -3 kb homologous recombination (HR) donor template were designed using the Benchling CRISPR Genome Engineering tool. The HR donor template was designed to introduce a 2 \times Flag-mAID tag in frame with the N terminus of *AMBRA1*, in the following order: methionine-FLAG-linker-FLAG-linker-mAID-linker-*AMBRA1*, and was purchased as a synthetic gene from Genewiz. For transient transfection, *AMBRA1* gRNA #3 (see Supplementary Table 4 for sequence details) were cloned into pSpCas9(BB)-2A-GFP (PX458), a gift from F. Zhang (Addgene plasmid #48138)²². Lentiviruses encoding gRNAs targeting human *AMBRA1* were subcloned into a Lenti-Guide-mCherry vector (see Supplementary Table 4 for sequence details). For *AMBRA1* knock-out in hTERT RPE-1, HCT-116, U-2 OS and T98G, cells were seeded into 10-cm dishes at approximately 70% confluency, and transfected with $5 \mu\text{g}$ of gRNA-containing PX458 plasmid, using Lipofectamine 3000 (Life Technologies). For 2 \times Flag-mAID-*AMBRA1* knockin, HCT-116 cells were seeded into 10-cm dishes at approximately 70% confluency, and transfected with $2.5 \mu\text{g}$ of gRNA-containing PX458 plasmid and $2.5 \mu\text{g}$ of HR donor template, using lipofectamine 3000 (Life Technologies). Two days after transfection, GFP-positive cells were sorted using the Beckman Coulter MoFlo XDP cell sorter (100- μm nozzle), and 15,000 cells were plated on a 15-cm dish. 8–10 days later, single cell clones were picked, dissociated in trypsin-EDTA (Sigma-Aldrich) for 5 min, and plated into individual wells of a 96-well plate for genotyping. Genomic DNA was collected using QuickExtract (Epicentre). Genotyping PCRs were performed with MyTaq HS Red Mix (Bioline), using primers

surrounding the genomic target sites (see Supplementary Table 4 for primer details). The resulting PCR products were then purified and sequenced to determine the presence of an insertion or deletion event. To further validate the mutational status of candidate clones, the PCR products were subjected to TOPO-TA Cloning (Invitrogen), and sequenced in order to distinguish the amplified products of distinct alleles. Fifty bacterial colonies for each TOPO-TA cloning reaction were sequenced and aligned to the corresponding wild-type template in Benchling to confirm that all alleles were correctly targeted. Clones positive to insertion or deletion events were then validated by western blot. For infection of BJAB and U-2932 cells, lentiviruses expressing either control sgRNA targeting luciferase or sgRNA targeting *AMBRA1* were produced in HEK 293T. After infection, mCherry-positive BJAB and U-2932 cells were selected by FACS and validated by western blot.

Immunofluorescence and live-cell microscopy

For immunofluorescence microscopy, cells were cultured on coverslips, washed in PBS, and fixed in 4% paraformaldehyde (PFA) in PBS for 10 min at room temperature. Cells were permeabilized with PBS/0.1% Triton X-100 for 10 min and blocked for 1 h in blocking buffer (PBS/0.05% Triton X-100 containing 5% FBS and 3% BSA) before incubation with the indicated primary antibodies in blocking buffer. Alexa-555 and Alexa-488-conjugated secondary antibodies were from Thermo Fisher Scientific and used at 1:2000 dilution. Slides were mounted in ProLong Diamond Antifade Mountant with DAPI (Thermo Fisher Scientific). Imaging was performed using a DeltaVision Elite inverted microscope system (Applied Precision), using a 60× objective (numerical aperture 1.42) from Olympus or a Zeiss LSM 800 microscope using a Plan-Apochromat 63×/1.40 oil objective. For live-cell microscopy, cells were seeded on Nunc LabTek II Chambered Coverglass 24 h before imaging. On the day of imaging, cells were incubated in FluoroBrite DMEM (Thermo Fisher Scientific) supplemented with 25 mM HEPES, 10% FBS (Corning Life Sciences) and 1% penicillin/streptomycin/L-glutamine (Corning Life Sciences). Imaging was performed using a DeltaVision Elite inverted microscope system (Applied Precision) with softWoRx (version 7.0.0), using a 60× objective (numerical aperture 1.42) from Olympus, or a Zeiss Axio Observer with Zeiss Zen (version 2.1), using an A-Plan 20× objective (numerical aperture 0.35) equipped with an Axio 506 monocular camera. To analyse changes in mean nuclear intensity, each nucleus was manually annotated by its starting frame (first frame in which a nucleus is visible), location at starting frame, and frame of initial PCNA foci formation. Tracking was then performed automatically by an in-house Python script. This script segments all objects in an image via thresholding and finds the closest object with a similar size and shape to the object identified in the image from the previous frame. The script continues until it can no longer identify any objects meeting the size–shape criteria within the distance cut-off. The tracks were outputted as movies for manual examination of their quality. Any nuclei where tracking failed or that were tracked for less than 10 h were excluded. The mean intensity for each nucleus at each time point was recorded during tracking. The tracks were aligned by setting the time of PCNA foci formation to 0 h for all tracks. The confidence intervals were calculated using the lineplot method of the Python package Seaborn, which uses the bootstrap method²³ to find the confidence interval. To measure cytoplasmic to nuclear intensity as a readout of CDK4/6 activity, ImageJ (version 1.52p) was used, as previously described²⁴.

Flow cytometry

For analysis of DNA replication, cells were pulsed with EdU (10 μM final concentration, Thermo Fisher Scientific) for 45 min, washed in PBS and fixed in 4% PFA. Detection of EdU was accomplished using the Click-iT Plus EdU Alexa Fluor 488 Flow Cytometry Assay Kit (Thermo Fisher Scientific) according to manufacturer's instructions. For analysis by flow cytometry, cells were counterstained with propidium iodide

(10 μg ml⁻¹ final concentration, Sigma-Aldrich) diluted in RNase (20 μg ml⁻¹ final concentration, Qiagen) containing PBS. Flow cytometry data were collected using the SP6800 Spectral Analyzer (Sony Biotechnology) using the SP6800 Spectral Analyzer software (version 1.6.3.7151). Flow cytometry data were analysed using the FlowJo software (version 10.7.1). A representative FACS gating strategy is provided in Supplementary Fig. 2.

In vitro ubiquitylation

C-terminal 3×Flag-tagged AMBRA1 was in vitro translated (IVT) using the TNT T7 Quick Coupled Transcription/Translation System (Promega) according to the manufacturer's recommendations. In vitro ubiquitylation reaction of synthetic phosphorylated (T286) cyclin D1 peptide (Yenzy) by 3×Flag-tagged AMBRA1 was carried out in buffer containing 50 mM Tris HCL pH 7.5, 5 mM MgCl₂, 1 mM DTT, 1 mM ATP, 0.1 μM E1 (Boston Biochem), 0.25 μM UBC H5C (Boston Biochem), 2.5 μM MG132, 0.2 nM okadaic acid, 0.2 μM NaV, and either 5 μM His-ubiquitin K0 (Boston Biochem) or 10 μM Myc-ubiquitin (Boston Biochem) and 3 μM ubiquitin aldehyde (Boston Biochem). Reactions were incubated at 30 °C for the indicated times, and terminated by adding NuPAGE LDS sample buffer (Thermo Fisher Scientific) followed by incubation for 5 min at 95 °C. Samples were resolved by SDS–PAGE and immunoblotted as indicated.

In vitro kinase assay

HEK 293T cells were transiently (co)transfected for 48 h with vectors expressing FFSS-tagged cyclin D1, FFSS-tagged cyclin D2, FFSS-tagged cyclin D3, HA-tagged CDK2, HA-tagged CDK4, or FH-tagged empty vector, in the combinations indicated. Complexes were purified by double immunoprecipitation in the following order: anti-Flag immunoprecipitation, elution with 3×Flag peptide, then anti-HA immunoprecipitation. Complexes bound to the beads were pre-washed in NEBuffer for Protein Kinases (PK, New England Biolabs B6022) and incubated with 0.5 μg human recombinant Rb (773-end) with an N-terminal GST tag, expressed in an *Escherichia coli* expression system (Sigma-Aldrich SRP0256). Reactions were carried out in NEBuffer for PK containing 0.1 mM NaV, 0.2 nM okadaic acid, 10 μM ATP in the presence or absence of either palbociclib isethionate (Sigma-Aldrich) or flavopiridol (Selleck Chemicals) at the concentrations indicated for 30 min at 30 °C, before stopping the reaction with Laemmli buffer. Samples were resolved by SDS–PAGE and immunoblotted as indicated.

Mouse and animal procedures

All animal work was performed following the ethical guidelines and protocols approved by the Institutional Animal Care and Use Committee of the University of Pennsylvania (IACUC Protocol 805157), and in accordance with the ethical international, EU and national formal approval obtained from the Danish Health Authorities (Dyreforsøgstilsynet, 2018-15-0201-01391) at the Danish Cancer Society Research Center. NSG mice were purchased from the Jackson Laboratory (Cat. No 005557). *Ambra1*^{tg/tg} mice were previously described⁷. To obtain *Ambra1*^{tg/tg} embryos, three- to six-month-old *Ambra1*^{tg/tg} mice were intercrossed, and vaginal plug inspection was carried out to determine the time of mating. For the assessment of morphological phenotypes and for immunofluorescence staining, abemaciclib mesylate (8 mg kg⁻¹, Selleck Chemicals) or PBS (vehicle) were administered from E8.5 to E13.5 by daily oral gavage using a disposable oral gavage needle. To measure abemaciclib by LC-MS/MS, abemaciclib mesylate was administered by daily oral gavage at two concentrations (8 mg kg⁻¹, 16 mg kg⁻¹) from E8.5 to E13.5, and at one concentration (100 mg kg⁻¹) from E12.5 to E13.5. Mice were sacrificed and the conceptuses from the gravid uteri were exposed to aspirate a sample of amniotic fluid for targeted LC-MS/MS analysis, using a 28G insulin syringe. The amniotic fluid samples were centrifuged at 2,700g for 10 min at 4 °C to remove cellular debris, and then stored at –80 °C for subsequent analysis. Maternal peripheral blood

Article

was collected by retro-orbital aspiration using heparinized capillary tubes (Thermo Fisher Scientific), and centrifuged at 2,700g for 10 min at 4 °C to separate the plasma fraction. Plasma was collected and stored at -80 °C for subsequent analysis. Maternal brains and embryonic tissue samples (mainly from the limbs) were collected, washed in PBS, and stored at -80 °C for subsequent analysis. For immunoblotting of brain lysates, E13.5 *Ambra1*^{+/+} and *Ambra1*^{tg/tg} mouse brain were collected and homogenized in lysis buffer (50 mM Tris-Cl pH 7.5, 320 mM sucrose, 10% glycerol, 1% NP-40) supplemented with protease inhibitors (Complete ULTRA, Roche) and phosphatase inhibitors (PhosSTOP, Roche).

Mass spectrometry for metabolomics

Amniotic fluid. For amniotic fluid samples, the abemaciclib extraction was carried out on each sample in a ratio of 50 µl sample per 1 ml of 50% methanol, 0.1% Trifluoroacetic acid (TFA). The sample in extraction buffer mixture was subjected to a homogenization step with zirconium disruption beads (0.5 mm, RPI) and homogenized for 10 min at 4 °C in a BeadBlaster with a 30 s on, 30 s off pattern. The homogenized sample was centrifuged at 21,000g for 3 min and a fixed volume of the supernatant (450 µl, all samples) was transferred to a 1.5-ml microfuge tube for speed vacuum concentration, no heating. The dried sample was then resuspended in 100% methanol (50 µl) for LC-MS analysis.

Plasma samples. For plasma samples, a solid phase extraction (SPE) procedure was used to extract abemaciclib and remove partial haemolysis products. The SPE cartridge (Hypersep SPE 500 mg/2.8 ml C18) was conditioned with 1 ml of 100% methanol, 0.1% TFA, and then equilibrated with 1 ml of HPLC grade water with 0.1% TFA. Then, 50 µl of plasma was homogenized with 950 µl of HPLC water with 0.1% TFA using the same method described above and a fixed volume of the homogenized mixture (900 µl) was loaded onto the SPE cartridge. Elution was carried out with two fractions (each 1 ml) of 50% methanol with 0.1% TFA. The two fractions for each sample were pooled and dried to completion by speed vacuum, then resuspended in 100% methanol and analysed by LC-MS.

Brain tissue. For the tissue samples, the abemaciclib extraction was carried out on each sample in a ratio of 50 mg per ml of HPLC grade water with 0.1% TFA, as with the plasma samples. After homogenization (same as for amniotic fluid and plasma), 300 µl of the sample mixture was then mixed with 700 µl of HPLC grade water with 0.1% TFA before loading. The rest of the SPE procedure was identical to the plasma SPE procedure described above.

Standard curve quantification. For both the amniotic fluid and plasma samples, an abemaciclib standard curve ranging from 10 nM to 1,000 nM was prepared in blank amniotic fluid (undosed controls) or blank plasma. These standard curve samples were extracted and analysed side-by-side with the experimental samples to account for matrix specific effects in the quantification. For tissue samples, no blank matrix control was suitable, so an external standard sample of abemaciclib in 100% methanol (1,000 nM) was used to confirm target detection. For the LC-MS analysis, three independent data acquisition sequences were carried out; plasma samples, amniotic fluid samples, and brain tissue samples. For each sequence, the order of acquisition (samples and standard curve points) was randomized to mitigate sequence bias, and each sample was preceded by a wash and blank injection to assess potential carryover. The sample data were interpolated against the respective standard curve in GraphPad Prism (v7.03).

Liquid chromatography. The LC column was an ACQUITY UPLC BEH Phenyl (1.0 × 50 mm, 1.7 µm) coupled to a Dionex Ultimate 3000 system and the column oven temperature was set to 25 °C for the gradient elution. A flow rate of 200 µl min⁻¹ was used with the following buffers: (A) HPLC-grade water with 0.1% formic acid, and (B) acetonitrile with 0.1%

formic acid. The gradient profile was as follows; 0–35% B (0–10 min), 35–75% B (10–15 min), 75–99% B (15–16.5 min), 99–0% B (16.5–16.75 min), 0–0% B (16.75–20 min). Injection volume was set to 1 µl for all analyses (20 min total run time per injection).

Mass spectrometry. MS analyses were carried out by coupling the LC system to a Thermo Q Exactive HF mass spectrometer operating in heated electrospray ionization mode. Method duration was 20 min with a polarity switching data-dependent Top 3 method for both positive and negative modes. A dedicated tandem MS (MS2) scan was programmed to target abemaciclib ($[M+2H]^{2+}$, 254.1432 *m/z*, isolation window of ± 0.2 *m/z*). Spray voltage for both positive and negative modes was 3.5 kV and capillary temperature was set to 320 °C with a sheath gas rate of 35, aux gas of 5. The full MS scan for both polarities used 120,000 resolution with an AGC target of 3×10^6 and a maximum IT of 100 ms, and the scan range was from 95–1,000 *m/z*. Tandem MS spectra for both positive and negative mode used a resolution of 15,000, AGC target of 1×10^5 , maximum IT of 50 ms, isolation window of 0.4 *m/z*, isolation offset of 0.1 *m/z*, and 3-way multiplexed normalized collision energies (nCE) of 10, 35, 80. The minimum AGC target was 5×10^4 with an intensity threshold of 1×10^6 . All data were acquired in profile mode.

Mass spectrometry imaging. Fresh frozen embryos were sectioned on a single slide at 10-µm thickness and thaw-mounted on conductive indium tin oxide IntelliSlides from Bruker Scientific. Slides were stored at -80 °C before analysis and dried in a vacuum desiccator before applying 2,5-dihydroxybenzoic acid MALDI matrix. Uniform layers of matrix were deposited in 12 spray passes over the tissue, at 15 mg ml⁻¹ in 70% acetonitrile + 0.1% TFA using the TM Sprayer from HTX Technologies. Data acquisition was performed with the dual source timsTOF Flex mass spectrometer from Bruker Scientific equipped with the 10kHz Smartbeam 3D laser and the dual trapped ion mobility separation cell. Detection settings were determined for abemaciclib using authentic standard (10 µM) spotted onto IntelliSlides and the MALDI MS/MS pattern was confirmed against the LC-MS/MS data: MALDI ionization mode $[M+H]^+$ at 507.2791 *m/z* (± 15 ppm) with a mobility (1/KO) of 1.177 (± 1%). Images of abemaciclib were acquired using FlexImaging software at 75-µm spatial resolution with M5 small laser profile and ScanBeam on, and the acquisition region was manually selected around the tissues using the registered optical image with a 1-mm border beyond the tissue. The ions generated in the MALDI source were separated in the trapped ion mobility cell using 90-ms ramp time and 100% duty cycle. Data analysis and visualization was performed in SciLS Lab software, FlexImaging and TIMS Data Viewer from Bruker Scientific. Tissue distribution of the drug and any isobaric molecules was visualized separately based on their specific mobility values (1/KO) extracted from TIMS Data Viewer. Data quality for each region was assessed using shared lipid features.

Immunofluorescence and haematoxylin and eosin staining

For immunofluorescent staining, embryos were fixed overnight in 4% PFA at 4 °C. Embryos were then washed three times in cold PBS, and dehydrated for cryopreservation in 30% sucrose in PBS at 4 °C, until sinking of the embryos. Upon full dehydration, embryos were moved to a 1:1 mixture of OCT compound (Thermo Fisher Scientific) and 30% sucrose/PBS, and gently rocked for 2 h. Embryos were then embedded in cryomolds that were pre-chilled in an isopentane (Sigma-Aldrich) bath on dry ice. Sections were obtained using a cryostat, re-hydrated in PBS, and blocked in 1× blocking buffer (Abcam) with 0.3% Triton X-100 for 1 h at room temperature in a humidified chamber. Primary antibodies were diluted in blocking buffer and incubated overnight at 4 °C. The following antibodies were used: cyclin D1 (1:200, Abcam ab16663), cyclin D2 (1:50, Santa Cruz Biotechnology sc-56305), KI67 (1:200, Abcam ab15580), and pRb (S807/811) (1:200, Cell Signaling Technology 8516S). Secondary antibodies were anti-rabbit (Alexa Fluor

488, Thermo Fischer Scientific A-11008) and anti-mouse (Alexa Fluor 555, Thermo Fischer Scientific A-21422), and used at 1:300 in 1× blocking buffer (Abcam) for 2 h at room temperature in a humidified chamber. Sections were then washed three times in PBS, incubated with DAPI in PBS for 10 min, and mounted with Fluoromount Aqueous Mounting Medium (Sigma-Aldrich). The signal-positive area for cyclin D1 and Ki67 intensity levels from the mesencephalic ventricular zone (MVZ) was quantified using ImageJ (version 1.52p) and normalized over the signal-positive area for DAPI intensity levels, setting the same intensity threshold among different conditions. For H&E staining, embryos were fixed overnight in 4% PFA at 4 °C. Embryos were then washed three times in cold PBS, and dehydrated in 30% sucrose in PBS at 4 °C, until sinking of the embryos. Upon full dehydration, embryos were moved to a 1:1 mixture of OCT compound (Thermo Fisher Scientific) and 30% sucrose/PBS, and gently rocked for 2 h. Embryos were then embedded in cryomolds that were pre-chilled in an isopentane (Sigma-Aldrich) bath on dry ice. Sections were obtained using a cryostat and rehydrated in PBS, followed by a wash in ddH₂O. Sections were then immersed in Gill's Haematoxylin No. 2 Solution (Bio-Optica, 05-06014/L) for 30 s. Sections were washed in ddH₂O, followed by 0.5% alcoholic eosin (Diapath, C0353). Sections were dehydrated with one, 10-s wash in 90% ethanol, and three, 10-s washes with 100% ethanol. Lastly, sections were immersed in Diasolv (Diapath, H0315) three times.

Immunohistochemistry of human tissues

Chromogenic immunohistochemistry for human *AMBRA1* was performed on plasma-thrombin cell blocks prepared from wild-type and knockout *AMBRA1* HCT-116 cell lines as previously described²⁵. Cell blocks were fixed in 10% Neutral Buffered formalin for 48 h, processed and paraffin embedded. Four-micrometre sections were collected from both cell blocks on to the same Plus microscope slides (Fisher Scientific Cat. No. 22-042-924) and stored at room temperature before use. Anonymized ovarian tumour tissue microarray (TMA) construction and sectioning was performed according to best practices²⁶. Unconjugated mouse anti-human *AMBRA1* clone G-6 (Santa Cruz Biotechnology sc-398204, lot no. G1217, RRID: AB_2861324), and unconjugated rabbit polyclonal anti-human *AMBRA1* (Proteintech Group 13762-1, lot no. 00005112 and 00017852, RRID: AB_10642007) were tested²⁷. Unconjugated rabbit anti-human cyclin D1 clone SP4 (Ventana Medical Systems 790-4508, lot no. B08078, RRID: AB_2335988) was used. Chromogenic immunohistochemistry was performed on a Ventana Medical Systems Discovery Ultra platform using Ventana's reagents and detection kits unless otherwise noted. Cyclin D1 (IVD) was used according to the manufacturer's instructions^{28,29}. *AMBRA1* antibodies were optimized by first determining antigen retrieval requirements followed by serial dilution of primary antibody to establish immunohistochemistry assay conditions. In brief, slides were deparaffinized online and endogenous peroxidase activity was blocked with 3% hydrogen peroxide for 4 min. Antigen retrieval for both *AMBRA1* antibodies was performed using Cell Conditioner 1 (Tris-EDTA pH8.5): 24 min at 95 °C for Santa Cruz Biotechnology and 48 min at 95 °C for Proteintech Group antibodies. Both antibodies were diluted 1:100 in Ventana antibody diluent (Ventana Medical Systems 760-018) and incubated for 12 and 6 h at room temperature, respectively. Primary antibody was detected using either goat anti-rabbit or goat anti-mouse horseradish peroxidase-conjugated multimer incubated for 8 min. The complex was visualized with 3,3 diaminobenzidine for 8 min and enhanced with copper sulfate for 4 min. All slides were washed in distilled water, counterstained with haematoxylin, dehydrated and mounted with permanent medium. Proteintech Group *AMBRA1* conditions were modified (increased primary time to 10 h and goat anti-mouse horseradish peroxidase conjugated multimer incubation to 12 min) and applied to the ovarian TMA. Analysis and scoring of the TMA was performed by either automated image analysis software (ImmunoRatio, version 1.0c)³⁰ for ImageJ (version 1.52o), or by visually determining the intensity of

nuclear immunoreactivity (0, no expression; 1, faint expression and 2, mild–moderate expression) for *AMBRA1*. Images were obtained using an Olympus BX43 microscope fitted with an Olympus DP27 camera using Olympus CellSens Entry (version 1.18).

Xenotransplantation experiments

Either female or male, eight-week-old NSG mice received subcutaneous flank injections of 1×10^7 BJAB or U-2932 cells that expressed control sgRNA targeting luciferase or sgRNA targeting *AMBRA1* (sgRNA#5) in 100 µl sterile PBS. Where indicated, mice were administered palbociclib isethionate (5 mg kg⁻¹ or 50 mg kg⁻¹ as indicated in Fig. 4; Selleckchem S1579) or PBS (as vehicle) via intraperitoneal injection for five consecutive days per week, until experimental end point. Treatment was started when tumours grew to 100 mm³. Experimental end point was considered when tumour volume reached 1,000 mm³ (U-2932) or exceeded 2,000 mm³ (BJAB), in accordance with the University of Pennsylvania IACUC guidelines. The institutional committee maximal tumour limits (4.2 cm³) were not exceeded. Tumour burden was monitored daily by palpation and visual inspection, and measured by caliper at the days indicated in the Source Data. Tumour volume was calculated as following: $V = (L \times W \times W)/2$, where V is tumour volume, L is tumour length and W is tumour width. Tumour weight was measured on the excised tumours at the experimental end point using an analytical scale.

Survival data analysis

To determine the association of *AMBRA1* expression with survival in human cancer, we performed survival analysis using Transcriptome Profiling data (HTSeq–FPKM) from all available cohorts in the TCGA database whose sample number is greater than or equal to 80 ($n = 10,547$). The expression and clinical data were directly downloaded using the TCGAbiolinks package (v2.12.6) in R (v3.6.0). The RNA expression data of *AMBRA1* was divided into high and low expression groups on the basis of either 20% or 50% quantiles. Kaplan–Meier survival curves analysis with log-rank testing were conducted and visualized using the survival package (v3.1) in R. In order to corroborate the survival data analysis from TCGA, we calculated a meta P value by combining the log-rank testing P values from each individual cohort analysed above, using the Fisher's method. The association of *AMBRA1* expression with survival in the diffuse large B-cell lymphoma (DLBCL) cohort was generated by combining the data from GEO accession GSE23501³¹ ($n = 69$) and GEO accession GSE10846³² ($n = 414$) downloaded from Oncomine (<https://www.oncomine.org>). To concatenate these two studies, we centre scaled the expression levels of *AMBRA1* using the Affymetrix probe '52731_at' for each study in R (scale function with the parameter centre = TRUE) and divided into high and low *AMBRA1* expression on the basis of 10% quantiles, individually. Survival analysis was then performed as in the above method.

Differential expression analysis

Differential expression analysis from TCGA (DLBC cohort, $n = 48$) was conducted between two groups of samples as previously described³³, and the list of the 300 most differentially expressed genes (two-sided Mann–Whitney U test, top and bottom 150 genes of the test statistics) was used to construct a heat map with the whole data set. Samples were clustered using the hierarchical clustering algorithm based on the complete linkage method and implemented on the Euclidean distance. Heat map and hierarchical clustering were generated and performed using the pheatmap package (v1.0.12) in R. Gene enrichment analysis of the differentially expressed genes was performed using Enrichr (<https://amp.pharm.mssm.edu/Enrichr/>) with BioPlant (2019), Reactome (2016) and NCI-Nature (2016) databases. Differential expression analyses of DLBCL patients from Compagno et al.³⁴ (Affymetrix probe '222189_at', $n = 64$) and Brune et al.³⁵ (Affymetrix probe '222189_at', $n = 36$) were generated in Oncomine (<https://www.oncomine.org>).

Correlation, mutation and methylation analyses

To determine the correlation between *AMBRA1* mRNA expression levels as measured by RNA-Seq (FPKM-UQ) and cyclin D1 protein expression levels as measured by reverse phase protein array (RPPA), we performed the Pearson correlation analysis across individual TCGA cohorts and plotted the figures using ggpubr package (v0.4.0) in R. OncoPrint map of the TCGA genetic alterations (DLBC cohort) was downloaded from cBioPortal (<https://www.cbioportal.org/>)^{36,37}. *CCND1*, *CCND2* and *CCND3* mutation profiles were gathered and combined from cBioPortal (curated set of non-redundant studies), COSMIC (<https://cancer.sanger.ac.uk/cosmic>)³⁸ and supplementary table 8 from Schmitz et al.³⁹. Redundant samples among the three data sets were removed by using their unique sample ID. Lollipop plots showing the amino acid position and its mutation numbers were generated using the ggplot2 package (v3.2.1) in R. *AMBRA1*, *FBXO11*, *CCNF* and *KEAP1* mutation profiles were downloaded from cBioPortal (curated set of non-redundant studies). CRISPR (Avana) Public 20Q1 pre-computed associations were downloaded from the Depmap portal (<https://depmap.org/portal/>). As a positive control for this method, we evaluated the dependencies of the genes encoding other established CRL substrate receptors that have a role in human cancer (that is, *CCNF*, *FBXW7*, *VHL* and *KEAP1*)^{40–43} and found that they inversely correlate with those of their substrates. Methylation data was downloaded from the TCGA (DLBC cohort) using SMART App (<http://www.bioinfo-zs.com/smartapp>)⁴⁴. CpG-aggregated methylation values (β -values, median aggregation method) were plotted in GraphPad Prism 8 (v8.3.1).

Statistical analyses

Data were analysed using GraphPad Prism 9.0.0 software, unless noted otherwise. Datasets were analysed using two-tailed statistical tests described in the figure legends.

Reporting summary

Further information on research design is available in the Nature Research Reporting Summary linked to this paper.

Data availability

All accession codes, unique identifiers, and web links for publicly available datasets are available within the article and in the Reporting Summary. Those who carried out the original analysis and collection of the data generated by the DECIPHER community bear no responsibility for the further analysis or interpretation of the data. Mass spectrometry data for cyclin D1 immunopurifications are provided in Supplementary Table 1. The full scanned images obtained by electrophoretic separation are provided in Supplementary Fig. 1. All original data are available from the corresponding authors upon request. Source data are provided with this paper.

Code availability

Custom scripts for image analysis are provided at GitHub (https://github.com/FenyoLab/CRL4AMBRA1_img_analysis). Custom scripts for cancer-related analyses are provided at GitHub (https://github.com/Lesdormis/AMBRA1_analysis).

- Sanjana, N. E., Shalem, O. & Zhang, F. Improved vectors and genome-wide libraries for CRISPR screening. *Nat. Methods* **11**, 783–784 (2014).
- Reynders, M. et al. PHOTACs enable optical control of protein degradation. *Sci. Adv.* **6**, eaay5064 (2020).
- Lee, J. & Zhou, P. DCAFs, the missing link of the CUL4–DDB1 ubiquitin ligase. *Mol. Cell* **26**, 775–780 (2007).
- Bern, M., Kil, Y. J. & Becker, C. Bionic: advanced peptide and protein identification software. *Curr. Protoc. Bioinformatics* **Chapter 13**, Unit13.20 (2012).
- Donato, V. et al. The TDH–GCN5L1–Fbxo15–KBP axis limits mitochondrial biogenesis in mouse embryonic stem cells. *Nat. Cell Biol.* **19**, 341–351 (2017).

- Jeong, Y. T. et al. The ULK1–FBXW5–SEC23B nexus controls autophagy. *eLife* **7**, e42253 (2018).
- Kuchay, S. et al. PTEN counteracts FBXL2 to promote IP3R3- and Ca²⁺-mediated apoptosis limiting tumour growth. *Nature* **546**, 554–558 (2017).
- Ran, F. A. et al. Genome engineering using the CRISPR–Cas9 system. *Nat. Protoc.* **8**, 2281–2308 (2013).
- Dragicevic, P. in *Modern Statistical Methods for HCI* (eds Robertson, J. & Kaptein, M.) 291–330 (Springer, 2016).
- Róna, G. et al. Dynamics of re-constitution of the human nuclear proteome after cell division is regulated by NLS-adjacent phosphorylation. *Cell Cycle* **13**, 3551–3564 (2014).
- Cecchetelli, A., Kwan, R., Krauter, S. & Chiriboga, L. Minimum concentration of cells required for the preparation of compact plasma-thrombin cell blocks. *J. Histotechnol.* **35**, 68–70 (2012).
- Glinsmann-Gibson, B. et al. Recommendations for tissue microarray construction and quality assurance. *Appl. Immunohistochem. Mol. Morphol.* (2020).
- Miki, Y. et al. *AMBRA1*, a novel α -synuclein-binding protein, is implicated in the pathogenesis of multiple system atrophy. *Brain Pathol.* **28**, 28–42 (2018).
- Lewitowicz, P. et al. Tumor digital masking allows precise triaging: a study based on Ki-67 scoring in gastrointestinal stromal tumors. *Scanning* **2018**, 7807416 (2018).
- Lorenzo-Martin, L. F. et al. VAV2 signaling promotes regenerative proliferation in both cutaneous and head and neck squamous cell carcinoma. *Nat. Commun.* **11**, 4788 (2020).
- Tuominen, V. J., Ruotoistenmäki, S., Viitanen, A., Jumppanen, M. & Isola, J. ImmunoRatio: a publicly available web application for quantitative image analysis of estrogen receptor (ER), progesterone receptor (PR), and Ki-67. *Breast Cancer Res.* **12**, R56 (2010).
- Shaknovich, R. et al. DNA methylation signatures define molecular subtypes of diffuse large B-cell lymphoma. *Blood* **116**, e81–e89 (2010).
- Lenz, G. et al. Molecular subtypes of diffuse large B-cell lymphoma arise by distinct genetic pathways. *Proc. Natl Acad. Sci. USA* **105**, 13520–13525 (2008).
- D'Angelo, F. et al. The molecular landscape of glioma in patients with Neurofibromatosis 1. *Nat. Med.* **25**, 176–187 (2019).
- Compagno, M. et al. Mutations of multiple genes cause deregulation of NF- κ B in diffuse large B-cell lymphoma. *Nature* **459**, 717–721 (2009).
- Brune, V. et al. Origin and pathogenesis of nodular lymphocyte-predominant Hodgkin lymphoma as revealed by global gene expression analysis. *J. Exp. Med.* **205**, 2251–2268 (2008).
- Cerami, E. et al. The cBio cancer genomics portal: an open platform for exploring multidimensional cancer genomics data. *Cancer Discov.* **2**, 401–404 (2012).
- Gao, J. et al. Integrative analysis of complex cancer genomics and clinical profiles using the cBioPortal. *Sci. Signal.* **6**, pii1 (2013).
- Tate, J. G. et al. COSMIC: the Catalogue Of Somatic Mutations In Cancer. *Nucleic Acids Res.* **47** (D1), D941–D947 (2019).
- Schmitz, R. et al. Burkitt lymphoma pathogenesis and therapeutic targets from structural and functional genomics. *Nature* **490**, 116–120 (2012).
- Clijsters, L. et al. Cyclin F controls cell-cycle transcriptional outputs by directing the degradation of the three activator E2Fs. *Mol. Cell* **74**, 1264–1277 (2019).
- Yada, M. et al. Phosphorylation-dependent degradation of c-Myc is mediated by the F-box protein Fbw7. *EMBO J.* **23**, 2116–2125 (2004).
- Maxwell, P. H. et al. The tumour suppressor protein VHL targets hypoxia-inducible factors for oxygen-dependent proteolysis. *Nature* **399**, 271–275 (1999).
- Kubbutat, M. H., Jones, S. N. & Vousden, K. H. Regulation of p53 stability by Mdm2. *Nature* **387**, 299–303 (1997).
- Li, Y., Ge, D. & Lu, C. The SMART app: an interactive web application for comprehensive DNA methylation analysis and visualization. *Epigenetics Chromatin* **12**, 71 (2019).
- Lin, D. I. et al. Phosphorylation-dependent ubiquitination of cyclin D1 by the SCF^{FBX4- α B-crystallin} complex. *Mol. Cell* **24**, 355–366 (2006).
- Okabe, H. et al. A critical role for FBXW8 and MAPK in cyclin D1 degradation and cancer cell proliferation. *PLoS ONE* **1**, e128 (2006).
- Santra, M. K., Wajapeyee, N. & Green, M. R. F-box protein FBXO31 mediates cyclin D1 degradation to induce G1 arrest after DNA damage. *Nature* **459**, 722–725 (2009).
- Wei, S. et al. A novel mechanism by which thiazolidinediones facilitate the proteasomal degradation of cyclin D1 in cancer cells. *J. Biol. Chem.* **283**, 26759–26770 (2008).
- Yu, Z. K., Gervais, J. L. & Zhang, H. Human CUL-1 associates with the SKP1/SKP2 complex and regulates p21(CIP1/WAF1) and cyclin D proteins. *Proc. Natl Acad. Sci. USA* **95**, 11324–11329 (1998).
- Chen, B. B., Glasser, J. R., Coon, T. A. & Mallampalli, R. K. FBXL2 is a ubiquitin E3 ligase subunit that triggers mitotic arrest. *Cell Cycle* **10**, 3487–3494 (2011).
- Chen, B. B. et al. F-box protein FBXL2 targets cyclin D2 for ubiquitination and degradation to inhibit leukemic cell proliferation. *Blood* **119**, 3132–3141 (2012).
- Pawar, S. A. et al. C/EBPdelta targets cyclin D1 for proteasome-mediated degradation via induction of CDC27/APC3 expression. *Proc. Natl Acad. Sci. USA* **107**, 9210–9215 (2010).
- Crooks, G. E., Hon, G., Chandonia, J. M. & Brenner, S. E. WebLogo: a sequence logo generator. *Genome Res.* **14**, 1188–1190 (2004).
- Yang, H. W. et al. Stress-mediated exit to quiescence restricted by increasing persistence in CDK4/6 activation. *eLife* **9**, e44571 (2020).
- Cappuccio, G., Ugga, L., Parrini, E., D'Amico, A. & Brunetti-Pierri, N. Severe presentation and complex brain malformations in an individual carrying a *CCND2* variant. *Mol. Genet. Genomic Med.* **7**, e708 (2019).
- Maini, I. et al. A novel *CCND2* mutation in a previously reported case of megalencephaly and perisylvian polymicrogyria with postaxial polydactyly and hydrocephalus. *Neuropediatrics* **49**, 222–224 (2018).
- McDermott, J. H. et al. Hypoglycaemia represents a clinically significant manifestation of PIK3CA- and *CCND2*-associated segmental overgrowth. *Clin. Genet.* **93**, 687–692 (2018).
- Mirzaa, G. et al. De novo *CCND2* mutations leading to stabilization of cyclin D2 cause megalencephaly-polymicrogyria-polydactyly-hydrocephalus syndrome. *Nat. Genet.* **46**, 510–515 (2014).
- Firth, H. V. et al. DECIPHER: Database of Chromosomal Imbalance and Phenotype in Humans Using Ensembl Resources. *Am. J. Hum. Genet.* **84**, 524–533 (2009).

60. Sameshima, T., Morisada, N., Egawa, T., Kugo, M. & Iijima, K. MPPH syndrome with aortic coarctation and macrosomia due to CCND2 mutations. *Pediatr. Int.* **62**, 115–117 (2020).

Acknowledgements We thank G. V. Pires, L. Moro, V. Donato, A. Zeke, A. Peschiaroli, M. Swartling, K. Avrampou, J. Wang, E. Hernandez and A. Tsirigos for their contribution to this work, and R. Abraham, S. Dann, K. Nakayama and W. Wei for critically reading the paper. This study makes use of data generated by the DECIPHER community. A full list of centres that contributed to the generation of the data is available from <https://decipher.sanger.ac.uk/about/stats> and via email from decipher@sanger.ac.uk. Funding for the DECIPHER project was provided by Wellcome. We thank E. Rosser and M. Lees from the Great Ormond Street Hospital for Children NHS Foundation Trust in London, UK, for providing the information on two patients with mutations in CCND2, deposited at DECIPHER (<https://decipher.sanger.ac.uk>). The Proteomics Laboratory, the Genome Technology Center (GTC), the Experimental Pathology Research Laboratory, the Cytometry and Cell Sorting Laboratory, and the Metabolomics Laboratory at NYU Langone Health are partially supported by the Cancer Center Support Grant P30CA016087 at the Laura and Isaac Perlmutter Cancer Center. The NYULH Center for Biospecimen Research and Development, Histology and Immunohistochemistry Laboratory (RRID:SCR_018304) is supported in part by the Laura and Isaac Perlmutter Cancer Center Support Grant, NIH/NCI P30CA016087, and the National Institutes of Health S10 Grants, NIH/ORIP S10OD01058 and S10OD018338. The authors thank C. I. Silvescu for data acquisition and processing of the mass spectrometry images. D.S. thanks F. Simoneschi, P. Simoneschi, D. Guidi and E. Guidi for continuous support. M.P. thanks T. M. Thor and T. B. Balduur for continuous support. This work was funded by grants from the National Institutes of Health (R01-CA76584 and R35-GM136250) to M.P. and (R01-CA207513-01) to L.B. The F.C. laboratory is supported by grants from the Danish Cancer Society (KBVU R72-A4408, R146-A9364, R231-A14034 to F.C. and R146-A9471 to V.C.), the Novo Nordisk Foundation (NNF13OC0007559, NNF16OC0022544), the Lundbeck Foundation (R233-2016-3360 to F.C. and R209-2015-3505 to V.C.), the LEO Foundation (LF17024 to F.C.), Associazione Italiana per la Ricerca sul Cancro (AIRC project IG 2019 no. 23543 to F.C.), the Italian Ministry of Research (MIUR, project PRIN

2017 Radius), and the Italian Ministry of Health (Ricerca Corrente to F.N.). V.C. is supported by Fondazione Umberto Veronesi. E.M. is an adjunct professor at UniCamillus—Saint Camillus International University of Health Sciences in Rome, Italy. F.B. is supported by a Young Investigator Grant from the Alex's Lemonade Stand Foundation. M.P. is an investigator with the Howard Hughes Medical Institute.

Author contributions D.S. conceived, planned and performed most experiments, and co-wrote the manuscript. G.R., Y.-T.J., A.O., A.A.W. and S.N. helped with biochemical experiments. N.Z. and L.B. performed the DLBCL xenografts. S.J. helped with bioinformatics analyses. F.B. helped with the collection of mouse plasma, embryos and amniotic fluid. S.K. and D.F. performed the automated analysis of live-cell images. Y.S. and D.R.J. performed the LC-MS/MS detection of abemaciclib. G.M., V.C., E.M., F.N. and F.C. performed the experiments with *Ambra1^{+/+}* and *Ambra1^{fl/fl}* mice related to neural development. A.A.A. analysed and scored immunohistochemistry stainings. M.P. conceived, directed and coordinated the study, oversaw the results and co-wrote the manuscript. All authors discussed the results and commented on the manuscript.

Competing interests M.P. is a consultant for and has financial interests in Coho Therapeutics, CullGen, Kymera Therapeutics and SEED Therapeutics. M.P. is a cofounder of Coho Therapeutics, and is a member of the scientific advisory board of CullGen, Kymera Therapeutics and SEED Therapeutics, and is a consultant for Santi Therapeutics. The other authors declare no competing interests.

Additional information

Supplementary information The online version contains supplementary material available at <https://doi.org/10.1038/s41586-021-03445-y>.

Correspondence and requests for materials should be addressed to L.B. or M.P.

Peer review information *Nature* thanks Piotr Sicinski and the other, anonymous, reviewer(s) for their contribution to the peer review of this work. Peer reviewer reports are available.

Reprints and permissions information is available at <http://www.nature.com/reprints>.